5

Parton branching and jet simulation

Complete perturbative calculations in QCD have been performed only to next-to-leading order in most cases, or to one further order in α_S for a few observables. The work involved increases roughly factorially with the order, so we cannot expect many more higher-order terms to be calculated soon. Nevertheless there are regions of phase space in which higher-order terms are enhanced and cannot be neglected. An example is the region of collinear parton emission from the struck parton in deep inelastic scattering. We saw in Section 4.3 that this region gives rise to logarithmic scaling violation in the structure functions. Another example is the high-thrust ($T \to 1$) region in e^+e^- annihilation, discussed in Section 3.4. Here the contribution of order α_S^n has a coefficient which is proportional to $\ln^{2n-1}(1-T)/(1-T)$ at large T. The extra factor of $\ln^2(1-T)$ for each power of α_S makes fixed-order predictions unreliable at high thrust.

In the present chapter we shall adopt a somewhat different approach from that of earlier chapters. Instead of aiming for a precise prediction to some fixed order in perturbation theory, we shall seek an approximate result in which such enhanced terms are taken into account to all orders. We shall see that this leads to a physically appealing 'parton shower' picture which can readily be implemented in computer simulations, often called QCD Monte Carlo programs. The parton shower represents an approximate perturbative treatment of QCD dynamics at scales of momentum transfer-squared t greater than some infra-red cut-off value t_0, typically taken to be of the order of 1 GeV^2. The Monte Carlo method is particularly convenient because the perturbative treatment at $t > t_0$ can be combined with a non-perturbative model of the hadronization process, assumed to take place at scales $t < t_0$. In this way one obtains a *QCD event generator*, *i.e.* a program which provides a complete model for a

Downloaded from https://www.cambridge.org/core. UNIVERSIDAD AUTONOMA METROPOLITANA, on 18 Nov 2026 at 04:36:53, subject to the Cambridge Core terms of use, available at https://www.cambridge.org/core/terms. https://doi.org/10.1017/CBO9780511628788.006

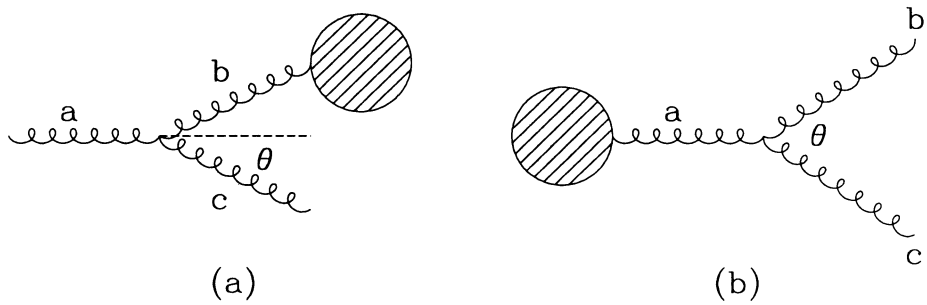


Fig. 5.1. Parton branching of (a) incoming and (b) outgoing partons.

given class of processes involving the interaction and/or production of hadrons.

Enhanced higher-order terms are associated with kinematic configurations for which the relevant QCD matrix elements are large. In particular, we have seen that there are enhancements when a soft gluon is emitted, or when a gluon or light quark splits into two almost collinear partons. The leading contributions of these soft and collinear configurations (and the corresponding enhanced virtual corrections) can be identified and summed to all orders, improving the convergence of the perturbation series.

We shall concentrate first on collinear enhancements, like those encountered in deep inelastic scattering. These are associated with *parton branching* on an incoming or outgoing line of a QCD Feynman diagram, as illustrated in Fig. 5.1. The shaded blobs represent the rest of the diagram, apart from the branching line, in this case a gluon. We shall calculate the contributions of such processes in some detail, because they form the basis not only for many tests of QCD but also for the QCD Monte Carlo programs mentioned above.

5.1 Parton branching

Fig. 5.2 shows the kinematics and notation for the branching of parton a into $b + c$. We assume that

$$p_b^2,\, p_c^2 \ll p_a^2 \equiv t \tag{5.1}$$

and for the moment we consider the case that a is an outgoing parton, which is called *timelike branching* since $t > 0$. The opening angle is $\theta = \theta_b + \theta_c$. Defining the energy fraction as

$$z = E_b/E_a = 1 - E_c/E_a\ , \tag{5.2}$$

Downloaded from https://www.cambridge.org/core. UNIVERSIDAD AUTONOMA METROPOLITANA, on 18 Nov 2026 at 04:36:53, subject to the Cambridge Core terms of use, available at https://www.cambridge.org/core/terms. https://doi.org/10.1017/CBO9780511628788.006

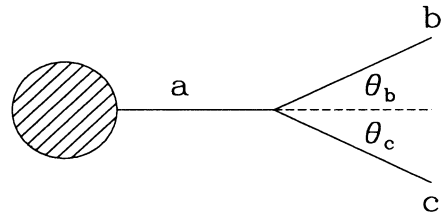


Fig. 5.2. Kinematics of timelike parton branching.

we have for small angles, where the matrix element is enhanced,

$$t = 2E_b E_c(1-\cos\theta) = z(1-z)E_a^2\theta^2 \,, \tag{5.3}$$

and hence, using transverse momentum conservation,

$$\theta = \frac{1}{E_a}\sqrt{\frac{t}{z(1-z)}} = \frac{\theta_b}{1-z} = \frac{\theta_c}{z} \,. \tag{5.4}$$

We consider first the case that all the partons a, b and c are gluons. There will be a factor in the amplitude proportional to $1/t$ from the propagator for gluon a, and a triple-gluon vertex factor

$$V_{ggg} = igf^{ABC}\varepsilon_a^\alpha \varepsilon_b^\beta \varepsilon_c^\gamma [g_{\alpha\beta}(p_a-p_b)_\gamma + g_{\beta\gamma}(p_b-p_c)_\alpha + g_{\gamma\alpha}(p_c-p_a)_\beta] \tag{5.5}$$

where ε_i^μ represents the polarization vector for gluon i. Note that here all momenta are defined as outgoing, so that $p_a = -p_b - p_c$. Using this and the conditions $\varepsilon_i \cdot p_i = 0$, we can write

$$V_{ggg} = -2igf^{ABC}[(\varepsilon_a\cdot\varepsilon_b)(\varepsilon_c\cdot p_b) - (\varepsilon_b\cdot\varepsilon_c)(\varepsilon_a\cdot p_b) - (\varepsilon_c\cdot\varepsilon_a)(\varepsilon_b\cdot p_c)] \,. \tag{5.6}$$

Since the three gluons are almost on mass-shell, we can take their polarization vectors to be purely transverse. We shall resolve them into plane polarization states, $\varepsilon_i^{\text{in}}$ in the plane of branching and $\varepsilon_i^{\text{out}}$ normal to the plane, as shown in Fig. 5.3, so that

$$\begin{aligned} \varepsilon_i^{\text{in}}\cdot\varepsilon_j^{\text{in}} &= \varepsilon_i^{\text{out}}\cdot\varepsilon_j^{\text{out}} = -1 \\ \varepsilon_i^{\text{in}}\cdot\varepsilon_j^{\text{out}} &= \varepsilon_i^{\text{out}}\cdot p_j = 0 \,. \end{aligned} \tag{5.7}$$

For small θ, neglecting terms of order θ^2, we have

$$\begin{aligned} \varepsilon_a^{\text{in}}\cdot p_b &= -E_b\theta_b = -z(1-z)E_a\theta \\ \varepsilon_b^{\text{in}}\cdot p_c &= +E_c\theta = (1-z)E_a\theta \\ \varepsilon_c^{\text{in}}\cdot p_b &= -E_b\theta = -zE_a\theta \,. \end{aligned} \tag{5.8}$$

Note that every vertex factor is proportional to θ, which, together with the $1/t \propto 1/\theta^2$ from the propagator, gives a $1/\theta$ singularity in the amplitude. Putting everything together using Eq. (5.4), we can write the matrix

Downloaded from https://www.cambridge.org/core. UNIVERSIDAD AUTONOMA METROPOLITANA, on 18 Nov 2026 at 04:36:53, subject to the Cambridge Core terms of use, available at https://www.cambridge.org/core/terms. https://doi.org/10.1017/CBO9780511628788.006

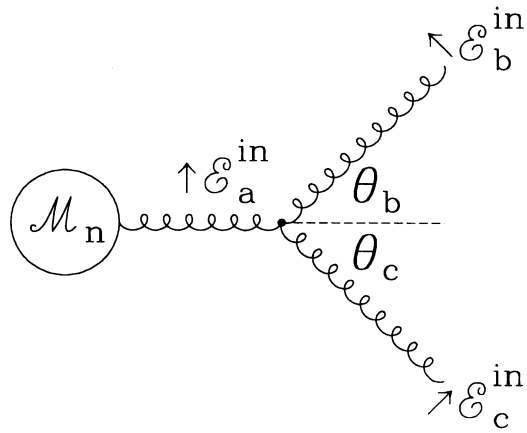


Fig. 5.3. Notation for $g \to gg$ branching.

ε_a	ε_b	ε_c	$F(z;\varepsilon_a,\varepsilon_b,\varepsilon_c)$
in	in	in	$(1-z)/z + z/(1-z) + z(1-z)$
in	out	out	$z(1-z)$
out	in	out	$(1-z)/z$
out	out	in	$z/(1-z)$

Table 5.1. Polarization dependence of the branching $g \to gg$.

element squared for $n+1$ partons in this small-angle region in terms of that for n partons,

$$|\mathcal{M}_{n+1}|^2 \sim \frac{4g^2}{t} C_A F(z;\varepsilon_a,\varepsilon_b,\varepsilon_c)\,|\mathcal{M}_n|^2 \tag{5.9}$$

where the colour factor $C_A = 3$ comes from $f^{ABC} f^{ABC}$ and the functions $F(z;\varepsilon_a,\varepsilon_b,\varepsilon_c)$ are given in Table 5.1.

All polarization combinations not given in Table 5.1 are forbidden. Defining $\langle F \rangle$ by averaging $F(z;\varepsilon_a,\varepsilon_b,\varepsilon_c)$ with respect to the polarization of a and summing over those of b and c, we find that

$$C_A \langle F \rangle \equiv \hat{P}_{gg}(z) = C_A \left[\frac{1-z}{z} + \frac{z}{1-z} + z(1-z) \right] \tag{5.10}$$

where $\hat{P}_{gg}(z)$ is called the unregularized *gluon splitting function* related to the corresponding Altarelli-Parisi kernel already encountered in Chapter 4.

We see from Table 5.1 that the enhancements in the matrix elements at $z \to 0$ (b soft) and $z \to 1$ (c soft) are associated with the emission of

Downloaded from https://www.cambridge.org/core. UNIVERSIDAD AUTONOMA METROPOLITANA, on 18 Nov 2026 at 04:36:53, subject to the Cambridge Core terms of use, available at https://www.cambridge.org/core/terms. https://doi.org/10.1017/CBO9780511628788.006

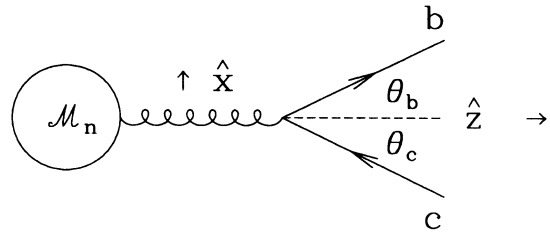


Fig. 5.4. Notation for $g \to q\bar{q}$ branching.

a soft gluon polarized in the plane of branching. Another important polarization effect is the correlation between the plane of branching and the polarization of the branching gluon. If we suppose that the polarization of gluon a is at an angle ϕ to the plane then the function F becomes

$$\begin{aligned} F_\phi &\propto \sum_{\epsilon_{b,c}} \left|\cos\phi\, \mathcal{M}(\varepsilon_a^{\text{in}}, \varepsilon_b, \varepsilon_c) + \sin\phi\, \mathcal{M}(\varepsilon_a^{\text{out}}, \varepsilon_b, \varepsilon_c)\right|^2 \\ &= \cos^2\phi \left[\frac{1-z}{z} + \frac{z}{1-z} + 2z(1-z)\right] + \sin^2\phi \left[\frac{1-z}{z} + \frac{z}{1-z}\right] \\ &= \frac{1-z}{z} + \frac{z}{1-z} + z(1-z) + z(1-z)\cos 2\phi\,. \end{aligned} \tag{5.11}$$

The first three terms give the unpolarized result and the last gives the correlation, which favours an orientation in which the polarization of the branching gluon lies in the plane of branching. The correlation is quite weak, however: its coefficient $z(1-z)$ vanishes in the enhanced regions $z \to 0, 1$ and reaches its maximum at $z = \frac{1}{2}$, where it is still only $1/9$ of the unpolarized contribution.

Consider next the branching of a gluon into a quark-antiquark pair, Fig. 5.4. Once again we have a factor of $1/t$ in the amplitude from the gluon propagator, but the vertex factor is now

$$V_{gq\bar{q}} = -ig\, t^A_{bc}\, \bar{u}^b \gamma_\mu \varepsilon_a^\mu v^c \tag{5.12}$$

where u^b and v^c are the quark and antiquark spinors. For this process we shall continue to use the plane polarization states defined above for the gluon, but will adopt helicity states for quarks and antiquarks. We follow the conventions of Bjorken and Drell [1] for spinors and Dirac algebra, in which

$$\gamma^0 = \begin{pmatrix} 1 & 0 \\ 0 & -1 \end{pmatrix}, \quad \gamma^i = \begin{pmatrix} 0 & \sigma_i \\ -\sigma_i & 0 \end{pmatrix} \tag{5.13}$$

where the matrix elements are themselves 2×2 matrices and σ_i are the Pauli spin matrices. Then to first order in small angles the helicity spinors

Downloaded from https://www.cambridge.org/core. UNIVERSIDAD AUTONOMA METROPOLITANA, on 18 Nov 2026 at 04:36:53, subject to the Cambridge Core terms of use, available at https://www.cambridge.org/core/terms. https://doi.org/10.1017/CBO9780511628788.006

ε_a	λ_b	λ_c	$F(z;\varepsilon_a,\lambda_b,\lambda_c)$
in	$\pm$	$\mp$	$(1-2z)^2$
out	$\pm$	$\mp$	1

Table 5.2. Polarization dependence of the branching $g \to q\bar{q}$.

are [1]

$$\begin{aligned} u_+^b &= \sqrt{E_b}\begin{pmatrix} 1 \\ \frac{1}{2}\theta_b \\ 1 \\ \frac{1}{2}\theta_b \end{pmatrix}, \quad u_-^b = \sqrt{E_b}\begin{pmatrix} -\frac{1}{2}\theta_b \\ 1 \\ \frac{1}{2}\theta_b \\ -1 \end{pmatrix}, \\ v_+^c &= i\sqrt{E_c}\begin{pmatrix} -\frac{1}{2}\theta_c \\ -1 \\ \frac{1}{2}\theta_c \\ 1 \end{pmatrix}, \quad v_-^c = i\sqrt{E_c}\begin{pmatrix} -1 \\ \frac{1}{2}\theta_c \\ -1 \\ \frac{1}{2}\theta_c \end{pmatrix}. \end{aligned} \tag{5.14}$$

Thus we find, for example,

$$-ig\bar{u}_+^b \gamma_\mu \varepsilon_a^{\text{in}\mu} v_-^c = \sqrt{E_b E_c}(\theta_b - \theta_c) = \sqrt{z(1-z)}(1-2z)E_a\theta\,, \tag{5.15}$$

and the matrix element relation analogous to Eq. (5.9) is

$$|\mathcal{M}_{n+1}|^2 \sim \frac{4g^2}{t} T_R F(z;\varepsilon_a,\lambda_b,\lambda_c)\,|\mathcal{M}_n|^2 \tag{5.16}$$

where the colour factor is now $\mathrm{Tr}(t^A t^A)/8 = T_R = 1/2$. The non-vanishing functions $F(z;\varepsilon_a,\lambda_b,\lambda_c)$ for quark and antiquark helicities λ_b and λ_c are given in Table 5.2.

In this case we see that the quark and antiquark helicities are always opposite, which is a consequence of the helicity conservation implied (for quarks of negligible mass) by the vector nature of the quark-gluon coupling. There are no soft ($z \to 0$ or 1) singularities since these are associated only with gluon emission. The spin-averaged splitting function is

$$T_R\langle F\rangle \equiv \hat{P}_{qg}(z) = T_R[z^2 + (1-z)^2]\,. \tag{5.17}$$

Note that in this case the amplitude vanishes at $z = \frac{1}{2}$ when the gluon a is polarized in the plane of branching, indicating a strong anticorrelation between the polarization and the plane. The angular correlation is now given by

$$\begin{aligned} F_\phi &\propto \cos^2\phi\,(1-2z)^2 + \sin^2\phi \\ &= z^2 + (1-z)^2 - 2z(1-z)\cos 2\phi\,. \end{aligned} \tag{5.18}$$

Downloaded from https://www.cambridge.org/core. UNIVERSIDAD AUTONOMA METROPOLITANA, on 18 Nov 2026 at 04:36:53, subject to the Cambridge Core terms of use, available at https://www.cambridge.org/core/terms. https://doi.org/10.1017/CBO9780511628788.006

λ_a	λ_b	ε_c	$F(z;\lambda_a,\lambda_b,\varepsilon_c)$
$\pm$	$\pm$	in	$(1+z)^2/(1-z)$
$\pm$	$\pm$	out	$1-z$

Table 5.3. Polarization dependence of the branching $q \to qg$.

Finally, for the branching in which a light quark (or antiquark) emits a gluon, the small-angle matrix element relation takes the form

$$|\mathcal{M}_{n+1}|^2 \sim \frac{4g^2}{t} C_F F(z;\lambda_a,\lambda_b,\varepsilon_c)\,|\mathcal{M}_n|^2 \tag{5.19}$$

with colour factor $C_F = \mathrm{Tr}(t^A t^A)/3 = 4/3$. All the necessary ingredients have been given in the previous two cases, and we leave it as an exercise for the reader to derive the results in Table 5.3 for the polarization dependent function $F(z;\lambda_a,\lambda_b,\varepsilon_c)$. The spin-averaged splitting function becomes

$$C_F \langle F \rangle \equiv \hat{P}_{qq}(z) = C_F \frac{1+z^2}{1-z}\,. \tag{5.20}$$

Notice that helicity conservation ensures that the quark does not change its helicity in this branching. Only the amplitude for gluon polarization in the plane of branching has the soft gluon ($z \to 1$) singularity: the 'out' amplitude actually vanishes at $z = 1$. Thus there is a preference for the gluon to be polarized in the plane, the angular correlation being given by

$$F_\phi \propto \frac{1+z^2}{1-z} + \frac{2z}{1-z}\cos 2\phi\,. \tag{5.21}$$

This angular correlation and those derived for the other branching processes are well illustrated by the angular distribution of four-jet events in e^+e^- annihilation, discussed in Chapter 3 and shown in Fig 3.11. Recall that the Bengtsson-Zerwas angle is the angle between the planes of the two hardest and two softest jets. The lowest-order Feynman diagrams contributing to four-jet production were given in Fig. 3.10. The two hardest jets tend to follow the directions of the quarks coming from the primary vertex, while the softer jets usually come from the produced quarks or gluons.

The three double bremsstrahlung diagrams in Fig. 3.10 give negligible correlations. The diagrams in which an emitted gluon splits into a quark-antiquark pair give a strong anti-correlation, as seen in the curve labelled 'Abelian' in Fig 3.11. This is because, as we have just seen, the gluon tends to be polarized in the plane of the primary jets and then prefers to split perpendicular to its polarization. On the other hand the splitting

Downloaded from https://www.cambridge.org/core. UNIVERSIDAD AUTONOMA METROPOLITANA, on 18 Nov 2026 at 04:36:53, subject to the Cambridge Core terms of use, available at https://www.cambridge.org/core/terms. https://doi.org/10.1017/CBO9780511628788.006

into two gluons occurs more often parallel to the polarization. Although the correlation is much weaker than that in $g \to q\bar{q}$, the two-gluon splitting is dominant in QCD, due to its larger colour factor and soft gluon enhancements. Thus the Bengtsson-Zerwas angular distribution is flatter than would be expected in an Abelian theory with no triple-boson vertex, in agreement with experiment.

In order to compute cross sections from the matrix elements for the various branching processes we have to consider also the initial-state flux factor $\mathcal{F}$ and the final-state n-parton phase space $d\Phi_n$:

$$d\sigma_n = \mathcal{F} \, |\mathcal{M}_n|^2 \, d\Phi_n \, . \tag{5.22}$$

For the timelike branching shown in Fig. 5.2, to go from the process with a outgoing to that in which it is replaced by $b + c$, we should replace

$$d\Phi_n = \ldots \frac{d^3\boldsymbol{p}_a}{2(2\pi)^3 E_a} \tag{5.23}$$

by

$$d\Phi_{n+1} = \ldots \frac{d^3\boldsymbol{p}_b}{2(2\pi)^3 E_b} \frac{d^3\boldsymbol{p}_c}{2(2\pi)^3 E_c} \, . \tag{5.24}$$

Now $p_c = p_a - p_b$ and hence $d^3\boldsymbol{p}_c = d^3\boldsymbol{p}_a$ at fixed p_b. Thus we find, in the usual small-angle approximation,

$$\begin{aligned} d\Phi_{n+1} &= d\Phi_n \frac{1}{2(2\pi)^3} \int E_b dE_b \, \theta_b d\theta_b \, d\phi \, dt \, \frac{dz}{1-z} \delta(t - E_b E_c \theta^2) \\ &\quad \delta(z - E_b/E_a) \\ &= d\Phi_n \frac{1}{4(2\pi)^3} dt \, dz \, d\phi \, , \end{aligned} \tag{5.25}$$

which gives

$$d\sigma_{n+1} = d\sigma_n \, \frac{dt}{t} \, dz \, \frac{d\phi}{2\pi} \, \frac{\alpha_S}{2\pi} \, CF \tag{5.26}$$

where C and F are respectively the colour factor and polarization dependent z-distribution introduced earlier. If we are not interested in the dependence on the azimuthal angle ϕ, we can make the replacement

$$\int \frac{d\phi}{2\pi} CF = \hat{P}_{ba}(z) \tag{5.27}$$

where $\hat{P}_{ba}(z)$ is the appropriate splitting function, to give

$$d\sigma_{n+1} = d\sigma_n \, \frac{dt}{t} \, dz \, \frac{\alpha_S}{2\pi} \, \hat{P}_{ba}(z) \, . \tag{5.28}$$

Finally let us consider the case of branching on an incoming line, as illustrated in Fig. 5.5, which is relevant to deep inelastic scattering. This

Downloaded from https://www.cambridge.org/core. UNIVERSIDAD AUTONOMA METROPOLITANA, on 18 Nov 2026 at 04:36:53, subject to the Cambridge Core terms of use, available at https://www.cambridge.org/core/terms. https://doi.org/10.1017/CBO9780511628788.006

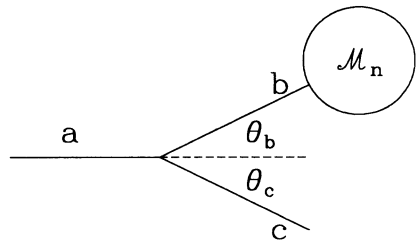


Fig. 5.5. Kinematics of spacelike parton branching.

branching will relate the process with b incoming to that with a incoming and c emitted. We can assume that

$$|p_a^2|\,,\; p_c^2 \ll |p_b^2| \equiv t \tag{5.29}$$

while as before $z = E_b/E_a = 1 - E_c/E_a$. Since the internal line has negative virtual mass-squared $-t$, this is called spacelike branching.

In the above treatment of the matrix elements for the various branching processes, we evaluated the vertex factors in the approximation that all lines were on mass-shell. Therefore the only changes we need to make in going from the timelike to the spacelike case are to the kinematics. For small angles we now have

$$t = E_a E_c \theta_c^2 \,. \tag{5.30}$$

Including the phase space for the emitted parton c at fixed E_b, we find

$$\begin{aligned} d\Phi_{n+1} &= d\Phi_n \frac{1}{2(2\pi)^3} \int E_c\, dE_c\, \theta_c\, d\theta_c\, d\phi\, dt\, dz\, \delta(t - E_a E_c \theta_c^2) \\ &\quad \delta(z - E_b/E_a) \\ &= d\Phi_n \frac{1}{4(2\pi)^3} dt\, \frac{dz}{z}\, d\phi \,. \end{aligned} \tag{5.31}$$

However, in this case we must remember that the initial-state flux factor $\mathcal{F}$ in Eq. (5.22) changes by a factor of z because of the change in energy of the incoming parton from E_b to E_a. Thus we find that Eqs. (5.26) and (5.28) also hold for spacelike branching.

5.2 Evolution equations

Next we consider the effect of multiple branching, that is, the enhancement of higher-order contributions associated with multiple small-angle parton emission. For the present we consider only a single type of branching, for example multiple gluon emission from a spacelike quark, as illustrated in Fig. 5.6. An incoming quark from the hadron A, initially with

Downloaded from https://www.cambridge.org/core. UNIVERSIDAD AUTONOMA METROPOLITANA, on 18 Nov 2026 at 04:36:53, subject to the Cambridge Core terms of use, available at https://www.cambridge.org/core/terms. https://doi.org/10.1017/CBO9780511628788.006

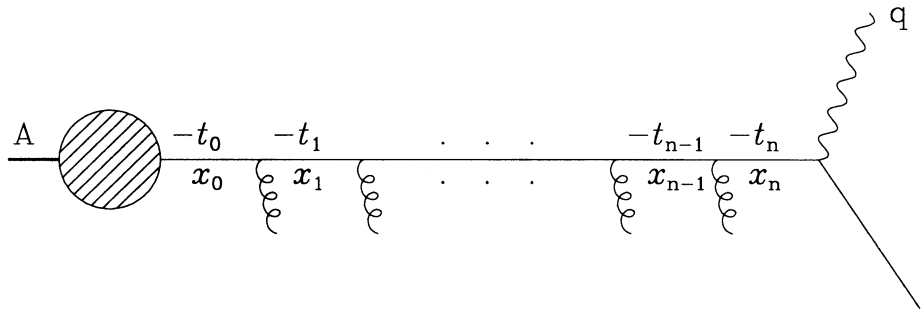


Fig. 5.6. Initial-state branching in deep inelastic lepton scattering.

a low virtual mass-squared $-t_0$ and carrying a fraction x_0 of the hadron's momentum, moves to more virtual masses and lower momentum fractions by successive small-angle emissions. Eventually it participates in a hard scattering process at a scale Q^2, for example deep inelastic lepton scattering, which involves the exchange of a photon of virtual mass-squared $q^2 = -Q^2$.

The cross section for the hard scattering process will depend on the scale Q^2 and on the momentum fraction distribution of the partons seen by the virtual photon at this scale, $f(x, Q^2)$. We can derive an evolution equation for the scale-dependence of this distribution, as follows. First we introduce a pictorial representation of the evolution, which will also prove useful later for discussing the Monte Carlo simulation of the process. We represent every sequence of branchings by a path in (t, x)-space. Two such paths are shown in Fig. 5.7. Each branching corresponds to a step downwards, from a higher to a lower value of the momentum fraction x, at a value of t equal to (minus) the virtual mass-squared after the branching. At $t = t_0$, the paths have some distribution of starting points $f(x_0, t_0)$ characteristic of the hadron A at that scale. Since the hard scattering sets an upper limit on the virtual mass scale of the struck parton, the distribution $f(x, t)$ of partons that would be seen at any scale t is just the x-distribution of paths at that scale.

Consider now the change in the parton distribution $f(x, t)$ when t is increased to $t+\delta t$. This is just the number of paths arriving in the element $(\delta t, \delta x)$ minus the number leaving that element, divided by δx. In the case illustrated in Fig. 5.7, there is one path arriving and one leaving. To find the total number arriving, we must integrate the branching probability times the parton density over all higher momentum fractions $x' = x/z$, to obtain

$$\delta f_{\text{in}}(x,t) \;=\; \frac{\delta t}{t}\int_x^1 dx'\,dz\frac{\alpha_S}{2\pi}\hat{P}(z)f(x',t)\,\delta(x-zx')$$

Downloaded from https://www.cambridge.org/core. UNIVERSIDAD AUTONOMA METROPOLITANA, on 18 Nov 2026 at 04:36:53, subject to the Cambridge Core terms of use, available at https://www.cambridge.org/core/terms. https://doi.org/10.1017/CBO9780511628788.006

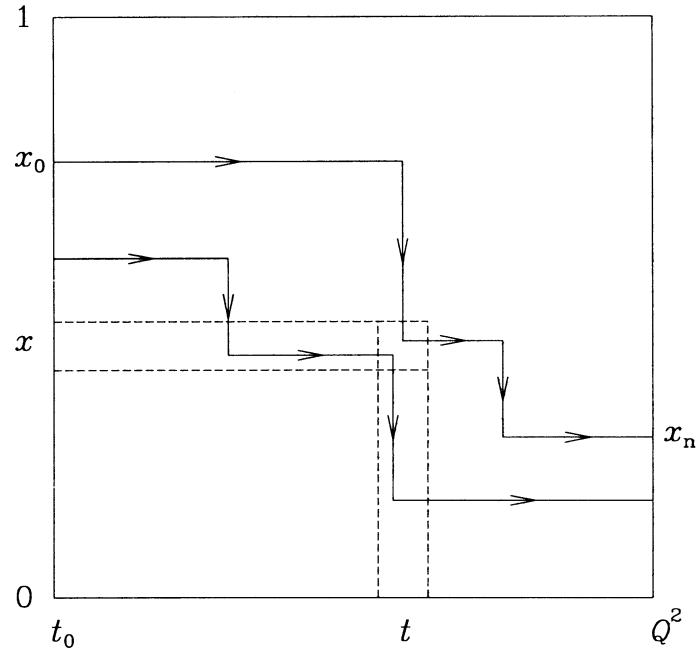


Fig. 5.7. Representation of parton branching by paths in (t, x)-space.

$$= \frac{\delta t}{t}\int_0^1 \frac{dz}{z}\frac{\alpha_S}{2\pi}\hat{P}(z)f(x/z,t) \tag{5.32}$$

where $\hat{P}(z)$ is the relevant unregularized splitting function. For quark splitting as in Fig. 5.6, $\hat{P}(z) = \hat{P}_{qq}(z)$, given by Eq. (5.20). The lower limit of the z-integration can be written as either zero or x because the integrand vanishes for $z < x$ $(x' > 1)$. For the number leaving the element, we integrate instead over all lower momentum fractions $x' = zx$:

$$\begin{aligned}\delta f_{\text{out}}(x,t) &= \frac{\delta t}{t}f(x,t)\int_0^x dx'\,dz\frac{\alpha_S}{2\pi}\hat{P}(z)\,\delta(x'-zx)\\ &= \frac{\delta t}{t}f(x,t)\int_0^1 dz\frac{\alpha_S}{2\pi}\hat{P}(z)\,.\end{aligned} \tag{5.33}$$

The net change in the population of the element is thus

$$\delta f(x,t) = \delta f_{\text{in}} - \delta f_{\text{out}} = \frac{\delta t}{t}\int_0^1 dz\,\frac{\alpha_S}{2\pi}\hat{P}(z)\left[\frac{1}{z}f(x/z,t) - f(x,t)\right]\,. \tag{5.34}$$

Using the plus prescription defined in Eq. (4.72), we can define the regularized splitting function

$$P(z) = \hat{P}(z)_+\,, \tag{5.35}$$

in terms of which the evolution equation for the parton density may be

Downloaded from https://www.cambridge.org/core. UNIVERSIDAD AUTONOMA METROPOLITANA, on 18 Nov 2026 at 04:36:53, subject to the Cambridge Core terms of use, available at https://www.cambridge.org/core/terms. https://doi.org/10.1017/CBO9780511628788.006

written as

$$t\frac{\partial}{\partial t}f(x,t) = \int_x^1 \frac{dz}{z}\frac{\alpha_S}{2\pi}P(z)f(x/z,t)\,. \tag{5.36}$$

We recognize Eq. (5.36) as the GLAP equation introduced in Chapter 4. The quantity $f(x,t)$ represents the distribution of parton momentum fractions inside the incoming hadron A probed at scale t. In the timelike branching of an outgoing parton, it can be used to represent instead the momentum fraction distribution of produced partons. The boundary conditions and direction of evolution are different, but the form of the evolution equation remains the same.

When there are several different types of partons in the branching process, we have to generalize the evolution equation to take into account the different processes by which a parton of type i can enter or leave the element $(\delta t, \delta x)$. This leads to a coupled set of evolution equations of the form

$$t\frac{\partial}{\partial t}f_i(x,t) = \sum_j \int_x^1 \frac{dz}{z}\frac{\alpha_S}{2\pi}P_{ij}(z)f_j(x/z,t)\,. \tag{5.37}$$

The regularized parton splitting functions $P_{ij}(z)$ can be derived as follows. A quark $(i = q)$ can enter the element either from the branching of a quark of the same flavour into quark-gluon, or from the splitting of a gluon into quark-antiquark. On the other hand, it can only leave the element via the process $q \to qg$. Thus the plus prescription applies only to that part, giving

$$\begin{aligned} P_{qq}(z) &= \hat{P}_{qq}(z)_+ = C_F\left(\frac{1+z^2}{1-z}\right)_+ \\ P_{qg}(z) &= \hat{P}_{qg}(z) = T_R\left[z^2+(1-z)^2\right]\,. \end{aligned} \tag{5.38}$$

For gluons $(i = g)$, things are a little more complicated. A gluon can arrive in the element either from $g \to gg$ or from $q \to qg$ (or $\bar{q} \to \bar{q}g$). In the first of these, either of the produced gluons can contribute. Thus Eq. (5.32) for the number arriving in the element becomes

$$\begin{aligned} \delta f_{g,\mathrm{in}}(x,t) &= \frac{\delta t}{t}\int_0^1 \frac{dz}{z}\frac{\alpha_S}{2\pi}\Big\{\hat{P}_{gg}(z)\left[f_g\left(\frac{x}{z},t\right)+f_g\left(\frac{x}{1-z},t\right)\right] \\ &\quad +\hat{P}_{qq}(z)\left[f_q\left(\frac{x}{1-z},t\right)+f_{\bar{q}}\left(\frac{x}{1-z},t\right)\right]\Big\} \\ &= \frac{\delta t}{t}\int_0^1 \frac{dz}{z}\frac{\alpha_S}{2\pi}\Big\{2\hat{P}_{gg}(z)f_g\left(\frac{x}{z},t\right) \\ &\quad +\hat{P}_{qq}(1-z)\left[f_q\left(\frac{x}{z},t\right)+f_{\bar{q}}\left(\frac{x}{z},t\right)\right]\Big\}\,, \end{aligned} \tag{5.39}$$

Downloaded from https://www.cambridge.org/core. UNIVERSIDAD AUTONOMA METROPOLITANA, on 18 Nov 2026 at 04:36:53, subject to the Cambridge Core terms of use, available at https://www.cambridge.org/core/terms. https://doi.org/10.1017/CBO9780511628788.006

where we have used the symmetry of $\hat{P}_{gg}(z)$, given by Eq. (5.10), under $z \to 1-z$. A gluon can leave the element by splitting into either gg or $q\bar{q}$ (with n_f possible flavours). The number leaving the element is thus

$$\delta f_{g,\mathrm{out}}(x,t) = \frac{\delta t}{t} f_g(x,t) \int_0^1 dz \frac{\alpha_S}{2\pi} \left[\hat{P}_{gg}(z) + n_f \hat{P}_{qg}(z)\, dz \right] . \qquad (5.40)$$

We can use the symmetry of $\hat{P}_{gg}(z)$ again to write

$$\int_0^1 \hat{P}_{gg}(z)\, dz = 2C_A \int_0^1 \left[\frac{z}{1-z} + \tfrac{1}{2} z(1-z) \right] dz , \qquad (5.41)$$

while from Eq. (5.17)

$$\int_0^1 \hat{P}_{qg}(z)\, dz = \frac{2}{3} T_R . \qquad (5.42)$$

We therefore find

$$\begin{aligned} P_{gg}(z) &= 2C_A \left[\left(\frac{z}{1-z} + \tfrac{1}{2} z(1-z) \right)_+ + \frac{1-z}{z} + \tfrac{1}{2} z(1-z) \right] \\ &\quad - \frac{2}{3} n_f T_R\, \delta(1-z) , \\ P_{gq}(z) &= P_{g\bar{q}}(z) = \hat{P}_{qq}(1-z) = C_F \frac{1+(1-z)^2}{z} . \end{aligned} \qquad (5.43)$$

Using the definition (4.72) of the plus prescription, one can easily check that

$$\begin{aligned} \left(\frac{z}{1-z} + \tfrac{1}{2} z(1-z) \right)_+ &= \frac{z}{(1-z)_+} + \tfrac{1}{2} z(1-z) + \frac{11}{12} \delta(1-z) \\ \left(\frac{1+z^2}{1-z} \right)_+ &= \frac{1+z^2}{(1-z)_+} + \frac{3}{2} \delta(1-z) , \end{aligned} \qquad (5.44)$$

and so the regularized splitting functions P_{qq} and P_{gg} can be written in the alternative forms

$$\begin{aligned} P_{qq}(z) &= C_F \left[\frac{1+z^2}{(1-z)_+} + \frac{3}{2} \delta(1-z) \right] \\ P_{gg}(z) &= 2C_A \left[\frac{z}{(1-z)_+} + \frac{1-z}{z} + z(1-z) \right] \\ &\quad + \frac{1}{6} (11 C_A - 4 n_f T_R)\, \delta(1-z) , \end{aligned} \qquad (5.45)$$

which coincide with the leading-order kernels given in Eq. (4.94). Notice that in both cases the singularity in the integrand of the evolution equations (5.37) at $z = 1$, corresponding to emission of a soft gluon, is removed by the plus prescription. The remaining singularity of P_{gg} at

Downloaded from https://www.cambridge.org/core. UNIVERSIDAD AUTONOMA METROPOLITANA, on 18 Nov 2026 at 04:36:53, subject to the Cambridge Core terms of use, available at https://www.cambridge.org/core/terms. https://doi.org/10.1017/CBO9780511628788.006

$z = 0$ is outside the region of integration ($x < z < 1$) and therefore all the integrals are finite.

The above formulation of the GLAP equations is convenient for obtaining analytical solutions for the evolution of parton distributions, as we have already seen in Chapter 4. To study more detailed features of the branching process, and in particular to say anything about the structure of the corresponding final states, a numerical approach based on the Monte Carlo simulation technique is useful. In this approach it is preferable to eliminate the plus prescription from the evolution equations, in the following way. For the moment we go back to the simplified treatment in which there is only one type of branching. We introduce the function

$$\Delta(t) \equiv \exp\left[-\int_{t_0}^{t} \frac{dt'}{t'} \int dz \, \frac{\alpha_S}{2\pi} \hat{P}(z)\right] , \tag{5.46}$$

which is called the *Sudakov form factor*. We shall see shortly that this function has a simple physical interpretation. Now we can write Eq. (5.34) as

$$t\frac{\partial}{\partial t} f(x,t) = \int \frac{dz}{z} \frac{\alpha_S}{2\pi} \hat{P}(z) f(x/z,t) + \frac{f(x,t)}{\Delta(t)} t\frac{\partial}{\partial t}\Delta(t) \tag{5.47}$$

and hence

$$t\frac{\partial}{\partial t}\left(\frac{f}{\Delta}\right) = \frac{1}{\Delta}\int \frac{dz}{z} \frac{\alpha_S}{2\pi} \hat{P}(z) f(x/z,t) \, . \tag{5.48}$$

Notice that this is similar in form to the Altarelli-Parisi equation (5.36), except that f is replaced by f/Δ and the regularized splitting function P is replaced by the unregularized one $\hat{P}$. This equation can be integrated to give an integral equation for $f(x,t)$ in terms of the initial parton distribution $f(x,t_0)$:

$$f(x,t) = \Delta(t) f(x,t_0) + \int_{t_0}^{t} \frac{dt'}{t'} \frac{\Delta(t)}{\Delta(t')} \int \frac{dz}{z} \frac{\alpha_S}{2\pi} \hat{P}(z) f(x/z,t') \, . \tag{5.49}$$

Equation (5.49) can be given a simple interpretation using the (t,x)-space paths depicted in Fig. 5.7. The first term on the right-hand side is the contribution from paths that do not branch between scales t_0 and t. Thus the Sudakov form factor $\Delta(t)$ is simply the probability of evolving from t_0 to t without branching. The second term is the contribution from all paths which have their last branching at scale t'. The factor of $\Delta(t)/\Delta(t')$ represents the probability of evolving from t' to t without branching. This is consistent with the above interpretation of $\Delta(t)$ because we see from Eq. (5.46) that $\Delta(t_0) = 1$.

The generalization of Eq. (5.46) to take account of several types of parton is straightforward. Each parton species i has its own form factor $\Delta_i(t)$, which describes its probability of evolving from t_0 to t without

Downloaded from https://www.cambridge.org/core. UNIVERSIDAD AUTONOMA METROPOLITANA, on 18 Nov 2026 at 04:36:53, subject to the Cambridge Core terms of use, available at https://www.cambridge.org/core/terms. https://doi.org/10.1017/CBO9780511628788.006

branching. Since the branching probability has to be summed over all possible processes $i \to j$, we have

$$\Delta_i(t) \equiv \exp\left[-\sum_j \int_{t_0}^{t} \frac{dt'}{t'} \int dz \, \frac{\alpha_S}{2\pi} \hat{P}_{ji}(z)\right] , \tag{5.50}$$

where $\hat{P}_{ji}(z)$ is the unregularized $i \to j$ splitting function. Correspondingly, Eq. (5.48) becomes

$$t\frac{\partial}{\partial t}\left(\frac{f_i}{\Delta_i}\right) = \frac{1}{\Delta_i} \sum_j \int \frac{dz}{z} \frac{\alpha_S}{2\pi} \hat{P}_{ij}(z) f_j(x/z, t) . \tag{5.51}$$

Our discussion of the Sudakov form factor up to this point has been somewhat schematic. We have ignored the infra-red singularity of the unregularized splitting functions at $z = 1$, which needs to be removed in order for the form factors to be defined.[1] In the form (5.37) of the evolution equations, the singularity is regularized by the plus prescription, but in the form (5.51) we must introduce an explicit infra-red cut-off, $z < 1 - \epsilon(t)$. Branchings with z above this range are classified as *unresolvable*: they involve the emission of an undetectably soft parton. The Sudakov form factor with this cut-off then gives the probability of evolving from t_0 to t without any *resolvable* branching.

Although we have not mentioned virtual corrections explicitly, the Sudakov form factor in fact sums enhanced virtual (parton loop) as well as real (parton emission) contributions to all orders. The virtual corrections affect the no-branching probability, and are included via unitarity, which is just the fact that the sum of the branching and no-branching probabilities must be unity. The resolvable branching probability tells us via unitarity the sum of the virtual and unresolvable real contributions: the latter two are both divergent but their sum is finite, and is included consistently in Eq. (5.51).

The definition of the infra-red cut-off $\epsilon(t)$ is to some extent a matter of choice about what we classify as a resolvable emission. For timelike branching, a natural resolution limit is provided by the cut-off on the parton virtual mass-squared, $t > t_0$. Working in a frame in which all the parton energies are much larger than their virtual masses, or equivalently defining z as the fraction of $p_+ = E + p_z$ with the z-axis along the momentum of parton a, the transverse momentum in the timelike branching $a \to bc$ is

$$p_T^2 = z(1-z)p_a^2 - (1-z)p_b^2 - zp_c^2 > 0 . \tag{5.52}$$

[1] The integrand $\hat{P}_{gg}(z)$ in the gluon form factor also has a singularity at $z = 0$ but this can be mapped to $z = 1$ using the symmetry property (5.41).

Downloaded from https://www.cambridge.org/core. UNIVERSIDAD AUTONOMA METROPOLITANA, on 18 Nov 2026 at 04:36:53, subject to the Cambridge Core terms of use, available at https://www.cambridge.org/core/terms. https://doi.org/10.1017/CBO9780511628788.006

Hence for $p_a^2 = t$ and $p_b^2, p_c^2 > t_0$ we require

$$z(1-z) > t_0/t \,, \tag{5.53}$$

that is,

$$z,\ 1-z > \epsilon(t) = \tfrac{1}{2} - \tfrac{1}{2}\sqrt{1-4t_0/t} \ \simeq\ t_0/t \,. \tag{5.54}$$

With such a cut-off, the Sudakov form factor of the quark, for example, becomes

$$\Delta_q(t) \simeq \exp\left[-\int_{2t_0}^{t} \frac{dt'}{t'} \int_{t_0/t'}^{1-t_0/t'} dz \frac{\alpha_S}{2\pi} \hat{P}_{qq}(z)\right] \,. \tag{5.55}$$

If we assume that the argument of the running coupling α_S is simply the virtual mass-squared scale t', this behaves at large t like

$$\left(\frac{t_0}{t}\right)^{p_1} \left(\frac{\alpha_S(t)}{\alpha_S(t_0)}\right)^{p_2} \tag{5.56}$$

where p_1 and p_2 are fixed powers. Thus, according to this assumption, the form factor vanishes roughly like a negative power of t at large t.

A more careful treatment of the running coupling suggests [2] that we should use as its argument $z(1-z)t'$, which from Eq. (5.52) is essentially the transverse momentum-squared. Expanding to next-to-leading order, we have

$$\alpha_S(z(1-z)t) = \alpha_S(t) + \beta_0 \ln[z(1-z)]\alpha_S^2(t)/4\pi + \cdots \,, \tag{5.57}$$

which, combined with a $1/(1-z)$ singularity in the splitting function $\hat{P}(z)$, produces a next-to-leading behaviour of the form $\ln(1-z)/(1-z)$ as $z \to 1$. This behaviour is indeed found in explicit higher-order calculations of the splitting functions P_{qq} and P_{gg}. The more singular behaviour near the cut-off in Eq. (5.55) then leads to a form factor that vanishes more rapidly at large t. Instead of (5.56) one finds

$$\Delta_q(t) \sim \left(\frac{\alpha_S(t)}{\alpha_S(t_0)}\right)^{p_3 \ln t} \,, \tag{5.58}$$

which tends to zero faster than any negative power of t.

In the spacelike branching $a \to bc$ it is the produced spacelike parton b that sets the largest scale $|p_b^2| = t > 0$. The kinematics again require that $1-z$, the momentum fraction carried by the emitted parton c with $p_c^2 > t_0$, should be greater than $\epsilon(t) \sim t_0/t$ at large t. A cut-off at small values of the momentum fraction z carried by parton b is not obligatory, since the value of z is in any case greater than x, the momentum fraction of the parton which participates in the hard subprocess (see Fig. 5.6). For simplicity one may take $z > t_0/t$, as in the timelike case.

Downloaded from https://www.cambridge.org/core. UNIVERSIDAD AUTONOMA METROPOLITANA, on 18 Nov 2026 at 04:36:53, subject to the Cambridge Core terms of use, available at https://www.cambridge.org/core/terms. https://doi.org/10.1017/CBO9780511628788.006

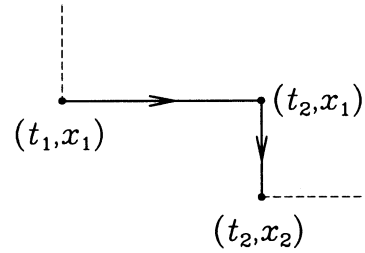


Fig. 5.8. Fundamental step in (t, x)-space.

The infra-red cut-offs that we have discussed in this section follow from kinematics and the constraint that each outgoing parton should have virtual mass-squared greater than t_0. In fact, however, the QCD branching picture that we have been using so far takes into account only amplitudes which have collinear enhancements. In the infra-red region there are also non-collinear amplitudes with enhancements due to soft gluon emission. We shall see in Section 5.5 that these interfere destructively in a way that effectively reduces the available phase space for parton branching, leading to more restrictive effective cut-offs than those defined above.

5.3 Monte Carlo method

The formulation of parton branching in terms of the Sudakov form factor is well suited to computer implementation, and is the basis of the 'parton shower' Monte Carlo programs for simulating QCD jets. We describe here the basic Monte Carlo branching algorithm in its simplest form, neglecting the complications of different possible branchings and QCD coherence effects. The former can be included straightforwardly using the formulae in the previous subsection. The latter will be the topic of the next subsection.

The basic problem that the Monte Carlo branching algorithm has to solve is as follows: given the virtual mass scale and momentum fraction (t_1, x_1) after some step of the evolution, or as initial conditions, generate the values (t_2, x_2) after the next step.

As shown in Fig. 5.8, the first quantity to be generated by the algorithm is the value of t_2. We saw above that the probability of evolving from t_1 to t_2 without (resolvable) branching is $\Delta(t_2)/\Delta(t_1)$ where $\Delta(t)$ is the Sudakov form factor. Thus t_2 can be generated with the correct probability distribution by solving the equation

$$\frac{\Delta(t_2)}{\Delta(t_1)} = \mathcal{R} \tag{5.59}$$

Downloaded from https://www.cambridge.org/core. UNIVERSIDAD AUTONOMA METROPOLITANA, on 18 Nov 2026 at 04:36:53, subject to the Cambridge Core terms of use, available at https://www.cambridge.org/core/terms. https://doi.org/10.1017/CBO9780511628788.006

where $\mathcal{R}$ is a random number distributed uniformly in the interval $[0, 1]$.[2]

If the value of t_2 is higher than the hard subprocess scale Q^2, this means that no further branching occurs (see Fig. 5.7). Otherwise, we have to generate the value of the momentum fraction $z = x_2/x_1$ for the next branching, with a probability distribution proportional to $(\alpha_S/2\pi)P(z)$, where $P(z)$ is the appropriate splitting function. We can do this by solving the equation

$$\int_{\epsilon}^{x_2/x_1} dz \frac{\alpha_S}{2\pi} P(z) = \mathcal{R}' \int_{\epsilon}^{1-\epsilon} dz \frac{\alpha_S}{2\pi} P(z) \tag{5.60}$$

where $\mathcal{R}'$ represents another random number in the interval $[0, 1]$ and ϵ is the infra-red cut-off for resolvable branching.

The above discussion applies to spacelike parton branching, as depicted in Fig. 5.6. The values of (t_i, x_i) generated by successive applications of the algorithm define the virtual masses and momentum fractions of the exchanged quark, from which the momenta of the emitted gluons can be computed. The azimuthal angles of their emission need to be specified by a further Monte Carlo algorithm, which in this case should generate the angles uniformly in the range $[0, 2\pi]$. More generally, for example when the exchanged spacelike parton is a gluon, the azimuths must be generated taking into account the polarization correlations discussed in Section 5.1.

Each emitted gluon in Fig. 5.6, and in general each parton with timelike momentum in a parton shower, can itself undergo further branching, which can be dealt with by a similar algorithm. The main difference in the timelike case is that t evolves *downwards* towards the cut-off value t_0 rather than upwards towards the hard process scale Q^2. The probability of evolving downwards without branching between t_1 and t_2 is $\Delta(t_1)/\Delta(t_2)$ and hence the equation corresponding to (5.59) in the timelike case is

$$\frac{\Delta(t_1)}{\Delta(t_2)} = \mathcal{R} \,. \tag{5.61}$$

Note that since $\Delta(t_0) = 1$ this equation has no solution for $t_2 > t_0$ if $\mathcal{R} < \Delta(t_1)$. This correctly generates the probability for no (resolvable) branching. If timelike branching does occur, the procedure for generating the momentum fraction z is the same as that described above for the spacelike case.

As a consequence of successive timelike branching, a *parton cascade* develops, as illustrated for e^+e^- annihilation in Fig. 5.9. Each outgoing

[2] If the form factor is known in closed form, Eq. (5.59) can be solved numerically, for example using Newton's method. Otherwise the values of the form factor can be tabulated and the solution obtained by interpolation.

Downloaded from https://www.cambridge.org/core. UNIVERSIDAD AUTONOMA METROPOLITANA, on 18 Nov 2026 at 04:36:53, subject to the Cambridge Core terms of use, available at https://www.cambridge.org/core/terms. https://doi.org/10.1017/CBO9780511628788.006

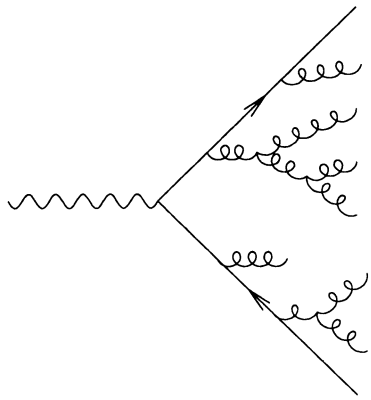


Fig. 5.9. Parton shower in e^+e^- annihilation.

line becomes the source of a new cascade, until the Monte Carlo algorithm generates a 'no branching' step in the evolution of its virtual mass. Those that do branch produce partons of lower virtual masses, which become more likely to generate no branching. Eventually all outgoing lines have stopped branching and the cascade ceases. At this stage, which depends on the cut-off scale t_0, the outgoing partons have to be converted into hadrons via a *hadronization model* if the Monte Carlo program is to be used for the simulation of real events. We shall discuss the different available models in Section 5.6.

5.4 Backward evolution

The branching algorithm described above generates what is known as *forward* evolution. At each step, a parton with timelike momentum is emitted and the emitting parton moves to a lower (more negative, in the spacelike case) virtual mass-squared. In Fig. 5.7, the initial momentum fraction x_0 of the emitting parton is known, but the final value x_n depends on the values of $z = x_{i+1}/x_i$ selected in the intervening steps. This is convenient in timelike evolution, such as that in e^+e^- annihilation, where we start with a quark and antiquark with $x_0 \simeq 1$ and generate a shower of partons with a range of momentum fractions. However, in spacelike cascades it is more convenient and efficient to start by specifying the momentum fraction x_n of the final parton, and then to generate $x_{n-1}, \ldots, x_0$ by *backward* evolution. This is because in this case it is the final partons, with the most negative virtual masses-squared, that participate in the hard subprocess.

In deep inelastic lepton scattering, for example, it is preferable to start by generating the hard lepton-quark scattering, which fixes the momen-

Downloaded from https://www.cambridge.org/core. UNIVERSIDAD AUTONOMA METROPOLITANA, on 18 Nov 2026 at 04:36:53, subject to the Cambridge Core terms of use, available at https://www.cambridge.org/core/terms. https://doi.org/10.1017/CBO9780511628788.006

tum fraction of the struck quark (neglecting its virtuality for the moment) at the Bjorken value $Q^2/2\nu$, as discussed in Chapter 4. Another important case is the Drell-Yan process for vector boson production in hadron-hadron collisions, to be considered in Chapter 9. In this process a quark from one incoming hadron and an antiquark from the other, with momentum fractions x_q and $x_{\bar{q}}$, collide to make a boson of mass M where $M^2 \simeq x_q x_{\bar{q}} s$, $\sqrt{s}$ being the hadron-hadron centre-of-mass energy. Thus we want the product of the final x_ns of the two spacelike partons to have just the right value in order to form a particular boson. If the cascades are generated forwards, then most of the time the product will not have the right value and the contribution to the cross section will be negligible, leading to a very low efficiency. If, on the other hand, we generate the initial-state cascades backwards, then we can choose an appropriate combination of momenta (and flavours) every time.

Efficient backward evolution cannot be achieved simply by running the forward evolution algorithm in reverse. For example, if one solves Eq. (5.60) for x_1 given x_2, then a fraction of the time one obtains $x_1 > 1$, which is unphysical. Thus naive backward evolution, like forward evolution, generates many configurations that have to be rejected, leading to low efficiency.

The correct prescription for backward evolution [3,4] involves the use of a modified form factor, which takes the local parton density $f(x,t)$ into account in choosing the next value of the evolution variable t. The probability of evolving backwards from (t_2, x) to (t_1, x) without branching is given by the function

$$\Pi(t_1, t_2; x) = \frac{f(x,t_1)\Delta(t_2)}{f(x,t_2)\Delta(t_1)} \,. \tag{5.62}$$

In other words, in place of the Sudakov form factor $\Delta(t_i)$ we should now use $\Delta(t_i)/f(x,t_i)$. The correct distribution of t_1 in the elementary backward step shown in Fig. 5.10 is then obtained by solving the equation

$$\Pi(t_1, t_2; x_2) = \mathcal{R} \tag{5.63}$$

where $\mathcal{R}$ is a random number distributed uniformly in the interval $[0,1]$.

When generating the corresponding value of the momentum fraction x_1, we have to multiply by the extra factor of $f(x_1,t_1)$ that will be divided out in the next backward step in t. Thus we have to generate $z = x_2/x_1$ with a probability distribution proportional to

$$\frac{\alpha_S}{2\pi}\frac{P(z)}{z} f(x_2/z, t_1) \tag{5.64}$$

where $P(z)$ is the appropriate splitting function. This can be done using a method similar to that used for the forward evolution, Eq. (5.60).

Downloaded from https://www.cambridge.org/core. UNIVERSIDAD AUTONOMA METROPOLITANA, on 18 Nov 2026 at 04:36:53, subject to the Cambridge Core terms of use, available at https://www.cambridge.org/core/terms. https://doi.org/10.1017/CBO9780511628788.006

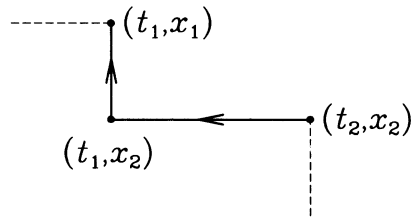


Fig. 5.10. Backward step in (t, x)-space.

To derive Eq. (5.62), let us define dF as the fraction of partons at (t_2, x) that came from branching between t and $t + dt$. Then the fraction that did not branch between t_1 and t_2 is

$$\Pi(t_1, t_2; x) = 1 - \int_{t_1}^{t_2} dF \,. \tag{5.65}$$

Now it follows from the evolution equation (5.49) that

$$\begin{aligned} f(x,t_2)dF &= \frac{dt}{t}\frac{\Delta(t_2)}{\Delta(t)}\int \frac{dz}{z}\frac{\alpha_S}{2\pi}\hat{P}(z)f(x/z,t) \\ &= dt\frac{\partial}{\partial t}\left[\frac{\Delta(t_2)}{\Delta(t)}f(x,t)\right] \,. \end{aligned} \tag{5.66}$$

Performing the integration in Eq. (5.65), we obtain the result (5.62).

In the original paper on this subject [3], the backward evolution form factor (5.62) was given in the apparently different form

$$\Pi(t_1, t_2; x) = \exp\left\{-\int_{t_1}^{t_2}\frac{dt}{t}\int\frac{dz}{z}\frac{\alpha_S}{2\pi}\hat{P}(z)\frac{f(x/z,t)}{f(x,t)}\right\} \,. \tag{5.67}$$

It is left as an exercise for the reader to show from the original form of the evolution equation, Eq. (5.34), that this is equivalent to Eq. (5.62).

The effect of the ratio of parton distributions in Eq. (5.62) is to suppress branching at large x, where $f(x,t)$ is a decreasing function of t, and to enhance it at low x, where $f(x,t)$ is increasing. This is correct because partons at higher x are less likely to have undergone branching, which always reduces the value of x. Similarly, the factor of $f(x_2/z, t_1)$ in the distribution of z suppresses branching from regions in which the parton density at $x_1 = x_2/z$ is low. In particular, it ensures that the selected value of x_1 is always less than unity.

We have presented the backward evolution algorithm for a single type of branching, *e.g.* $q \to qg$. As was the case for the evolution equations (5.37), it is straightforward to generalize the above treatment by attaching the appropriate labels to the splitting functions, form factors and parton distributions.

Downloaded from https://www.cambridge.org/core. UNIVERSIDAD AUTONOMA METROPOLITANA, on 18 Nov 2026 at 04:36:53, subject to the Cambridge Core terms of use, available at https://www.cambridge.org/core/terms. https://doi.org/10.1017/CBO9780511628788.006

One difference between forward and backward evolution is that the former may be used as a way of solving the GLAP equations (5.37), to obtain the t-dependence of the parton distributions. In backward evolution, the parton distributions are part of the input: they are used to 'guide' the evolution paths towards the most populated regions of (t, x)-space. The primary aim is to generate the correct distribution of the partons emitted in the initial-state cascade.

5.5 Coherent branching

So far in this Chapter we have been developing a parton branching formalism which takes account of collinear enhancements to all orders in perturbation theory. In addition, there are enhancements associated with soft gluon emission. We have seen evidence of these in the singularities of the small-angle parton splitting functions for soft gluon emission, but they are more general. Whenever an external line of a QCD Feynman graph with momentum p and mass m (not necessarily small) emits a gluon of momentum q, there is a propagator factor of

$$\frac{1}{(p \pm q)^2 - m^2} = \frac{\pm 1}{2p \cdot q} = \frac{\pm 1}{2\omega E(1 - v\cos\theta)} \tag{5.68}$$

where ω is the energy of the gluon, E and v the energy and velocity of the parton emitting it, and θ the angle of emission. For light partons $v \to 1$ and we have a collinear enhancement as $\theta \to 0$. However, there is also an enhancement as $\omega \to 0$ for any velocity and emission angle.

The soft enhancement corresponds to a colour factor times a universal, spin-independent factor of

$$F_{\text{soft}} = \frac{p \cdot \varepsilon}{p \cdot q} \tag{5.69}$$

in the amplitude, where ε is the polarization vector of the emitted gluon. In the case of emission from a quark, for example, apart from the factor of $1/2p \cdot q$ there is a numerator factor of the form $N \cdot \varepsilon$, where, as $\omega \to 0$,

$$\begin{aligned} N^\mu &= (\not{p} + \not{q} + m)\gamma^\mu u(p) \\ &\to (\gamma^\nu \gamma^\mu p_\nu + \gamma^\mu m)u(p) \\ &= (2p^\mu - \gamma^\mu \not{p} + \gamma^\mu m)u(p) \\ &= 2p^\mu u(p)\,. \end{aligned} \tag{5.70}$$

In the last step we have used the Dirac equation for the on-mass-shell spinor $u(p)$. The universal factor F_{soft} corresponds to the classical *eikonal formula* for the radiation from a current p^μ, which is valid in the long-wavelength limit.

Downloaded from https://www.cambridge.org/core. UNIVERSIDAD AUTONOMA METROPOLITANA, on 18 Nov 2026 at 04:36:53, subject to the Cambridge Core terms of use, available at https://www.cambridge.org/core/terms. https://doi.org/10.1017/CBO9780511628788.006

Notice that there is no soft enhancement of radiation from an off-mass-shell internal line of a Feynman graph, since the associated denominator factor $(p+q)^2 - m^2 \to p^2 - m^2 \neq 0$ as $\omega \to 0$.

An enhancement factor in the amplitude for each external line implies that the cross section has a factor which is a sum over all pairs of external lines $\{i, j\}$:

$$d\sigma_{n+1} = d\sigma_n \frac{d\omega}{\omega} \frac{d\Omega}{2\pi} \frac{\alpha_S}{2\pi} \sum_{i,j} C_{ij} W_{ij} \tag{5.71}$$

where $d\Omega$ is the element of solid angle for the emitted gluon, C_{ij} is a colour factor to be computed, and the *radiation function* W_{ij} is given by

$$W_{ij} = \frac{\omega^2 p_i \cdot p_j}{p_i \cdot q \, p_j \cdot q} = \frac{1 - v_i v_j \cos\theta_{ij}}{(1 - v_i \cos\theta_{iq})(1 - v_j \cos\theta_{jq})} \,. \tag{5.72}$$

The colour-weighted sum of radiation functions in Eq. (5.71) is sometimes called the *antenna pattern* of the process.

Although the radiation function (5.72) represents an interference contribution from lines i and j, it can be separated into two parts containing the leading collinear singularities. For simplicity we consider here the case of massless emitting particles, $v_i = v_j = 1$. Then we can write

$$W_{ij} = W_{ij}^{[i]} + W_{ij}^{[j]} \tag{5.73}$$

where

$$W_{ij}^{[i]} = \frac{1}{2} \left(W_{ij} + \frac{1}{1 - \cos\theta_{iq}} - \frac{1}{1 - \cos\theta_{jq}} \right) \,. \tag{5.74}$$

The function (5.74) has a remarkable property known as *angular ordering*. Suppose we write the angular integration in Eq. (5.71) in terms of polar and azimuthal angles with respect to the direction of line i,

$$d\Omega = d\cos\theta_{iq} \, d\phi_{iq} \,, \tag{5.75}$$

and then carry out the azimuthal integration. We find that

$$\begin{aligned} \int_0^{2\pi} \frac{d\phi_{iq}}{2\pi} W_{ij}^{[i]} &= \frac{1}{1 - \cos\theta_{iq}} \quad \text{if } \theta_{iq} < \theta_{ij} \\ &= 0 \qquad \text{otherwise.} \end{aligned} \tag{5.76}$$

In other words, after azimuthal averaging, the contribution from this term is confined to a cone, centred on the direction of line i, extending in angle as far as the direction of line j. Similarly, the contribution $W_{ij}^{[j]}$, after averaging over ϕ_{jq}, is confined to a cone centred on line j extending as far as line i.

To prove the angular ordering property of $W_{ij}^{[i]}$, we note that

$$1 - \cos\theta_{jq} = a - b\cos\phi_{iq} \tag{5.77}$$

Downloaded from https://www.cambridge.org/core. UNIVERSIDAD AUTONOMA METROPOLITANA, on 18 Nov 2026 at 04:36:53, subject to the Cambridge Core terms of use, available at https://www.cambridge.org/core/terms. https://doi.org/10.1017/CBO9780511628788.006

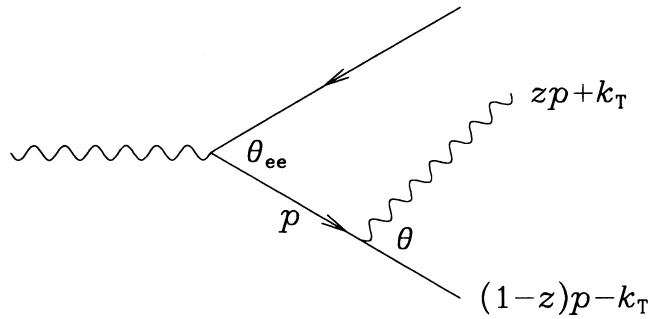


Fig. 5.11. Soft photon emission from an electron-positron pair.

where

$$a = 1 - \cos\theta_{ij}\cos\theta_{iq}\ , \quad b = \sin\theta_{ij}\sin\theta_{iq}\ . \tag{5.78}$$

Defining $z = \exp(i\phi_{iq})$, we have

$$I_{ij}^{[i]} \equiv \int_0^{2\pi} \frac{d\phi_{iq}}{2\pi} \frac{1}{1-\cos\theta_{jq}} = \frac{1}{i\pi b} \oint \frac{dz}{(z-z_+)(z-z_-)} \tag{5.79}$$

where the z-integration contour is the unit circle and

$$z_\pm = \frac{a}{b} \pm \sqrt{\frac{a^2}{b^2} - 1}\ . \tag{5.80}$$

Now only the pole at $z = z_-$ can lie inside the unit circle and therefore

$$I_{ij}^{[i]} = \sqrt{\frac{1}{a^2-b^2}} = \frac{1}{|\cos\theta_{iq} - \cos\theta_{ij}|}\ . \tag{5.81}$$

Hence

$$\int_0^{2\pi} \frac{d\phi_{iq}}{2\pi} W_{ij}^{[i]} = \frac{1}{2(1-\cos\theta_{iq})}\left[1 + (\cos\theta_{iq} - \cos\theta_{ij}) I_{ij}^{[i]}\right]\ , \tag{5.82}$$

which gives Eq. (5.76).

The angular ordering property of soft emission is an example of a coherence effect common to all gauge theories. In electrodynamics it accounts for the suppression of soft bremsstrahlung from electron-positron pairs (called the *Chudakov effect*), which has a simple heuristic explanation in terms of old-fashioned time-ordered perturbation theory. Consider the emission of a soft photon at angle θ from an electron in a pair with opening angle $\theta_{ee} < \theta$, as shown in Fig. 5.11.

For simplicity we shall assume $\theta_{ee}, \theta \ll 1$. Then the transverse momentum of the photon is $k_T \sim zp\theta$ and the energy imbalance at the $e \to e\gamma$ vertex is

$$\Delta E \sim k_T^2/zp \sim zp\theta^2\ . \tag{5.83}$$

Downloaded from https://www.cambridge.org/core. UNIVERSIDAD AUTONOMA METROPOLITANA, on 18 Nov 2026 at 04:36:53, subject to the Cambridge Core terms of use, available at https://www.cambridge.org/core/terms. https://doi.org/10.1017/CBO9780511628788.006

According to the uncertainty principle the time available for the photon emission is $\Delta t \sim 1/\Delta E$. In this time interval the transverse separation of the pair will become $\Delta b \sim \theta_{ee}\Delta t$. In order for there to be a non-negligible probability of photon emission, the photon must be able to resolve this transverse separation. This will be the case if

$$\Delta b > \lambda/\theta \sim (zp\theta)^{-1} \tag{5.84}$$

where λ is the photon wavelength. However, this implies that

$$\theta_{ee}(zp\theta^2)^{-1} > (zp\theta)^{-1} , \tag{5.85}$$

and hence that $\theta_{ee} > \theta$. Thus soft photon emission is suppressed at angles larger than the opening angle of the pair. Photons at larger angles cannot resolve the individual electron and positron charges and see only the net charge of the system, which in this case is zero, implying no emission.

The only complication in going from electro- to chromodynamics is that the electric charges are replaced by colour charges. In a suitable representation of the colour algebra, we can represent the colour charge of particle i by a vector $\boldsymbol{Q}_i$ such that $\boldsymbol{Q}_i^2 = C_F = 4/3$ for a quark, $\boldsymbol{Q}_i^2 = C_A = 3$ for a gluon and $\boldsymbol{Q}_i^2 = 0$ for a colour singlet. In this notation, the colour factor in Eq. (5.71) is

$$C_{ij} = -\boldsymbol{Q}_i \cdot \boldsymbol{Q}_j . \tag{5.86}$$

For two external lines forming a colour singlet, as in $e^+e^- \to q\bar{q}$ for example, we have $\boldsymbol{Q}_i + \boldsymbol{Q}_j = 0$ and hence $C_{ij} = \boldsymbol{Q}_i^2 = \boldsymbol{Q}_j^2$. In this case the angular ordering operates as in electrodynamics, suppressing radiation outside the cones extending from i to j and vice-versa.

A more interesting case is that of three partons (i, j, k) forming a colour singlet, as in $e^+e^- \to q\bar{q}g$. The soft gluon radiation pattern will be determined by the expression

$$\begin{aligned} W &= -\boldsymbol{Q}_i \cdot \boldsymbol{Q}_j W_{ij} - \boldsymbol{Q}_j \cdot \boldsymbol{Q}_k W_{jk} - \boldsymbol{Q}_i \cdot \boldsymbol{Q}_k W_{ik} \\ &= \tfrac{1}{2}\Big[\boldsymbol{Q}_i^2(W_{ij} + W_{ik} - W_{jk}) + \boldsymbol{Q}_j^2(W_{ij} + W_{jk} - W_{ik}) \\ &\quad + \boldsymbol{Q}_k^2(W_{ik} + W_{jk} - W_{ij})\Big] . \end{aligned} \tag{5.87}$$

Let us study in detail the configuration in which i and j are close in angle, forming a system l with colour charge $\boldsymbol{Q}_l = \boldsymbol{Q}_i + \boldsymbol{Q}_j = -\boldsymbol{Q}_k$, as depicted in Fig. 5.12. Using the decomposition (5.73), we can write Eq. (5.87) in the form

$$\begin{aligned} W &= \boldsymbol{Q}_i^2(W_{ij}^{[i]} + \tilde{W}_{jk}^{[i]} - \tilde{W}_{ik}^{[j]}) + \boldsymbol{Q}_j^2(W_{ij}^{[j]} + \tilde{W}_{ik}^{[j]} - \tilde{W}_{jk}^{[i]}) \\ &+ \boldsymbol{Q}_k^2(\tilde{W}_{jk}^{[i]} + \tilde{W}_{ik}^{[j]} + \tfrac{1}{2}W_{ik}^{[k]} + \tfrac{1}{2}W_{jk}^{[k]}) \end{aligned} \tag{5.88}$$

Downloaded from https://www.cambridge.org/core. UNIVERSIDAD AUTONOMA METROPOLITANA, on 18 Nov 2026 at 04:36:53, subject to the Cambridge Core terms of use, available at https://www.cambridge.org/core/terms. https://doi.org/10.1017/CBO9780511628788.006

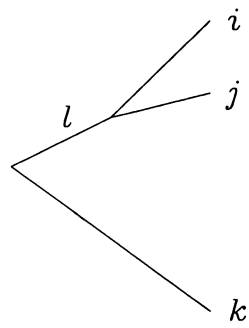


Fig. 5.12. Soft gluon emission from a three-parton system.

where

$$\tilde{W}_{jk}^{[i]} = \tfrac{1}{2}(W_{ik}^{[i]} - W_{ij}^{[i]}) \,, \quad \tilde{W}_{ik}^{[j]} = \tfrac{1}{2}(W_{jk}^{[j]} - W_{ij}^{[j]}) \,. \tag{5.89}$$

Note that the collinear singularities along the directions of i and j are cancelled in the expressions (5.89). Since the angle between i and j is small, we can approximate the direction of i or j by that of l in all functions that are not singular in the directions of i or j. Thus we can write

$$\begin{aligned} W_{ik}^{[k]} &\simeq W_{jk}^{[k]} \simeq W_{lk}^{[k]} \\ \tilde{W}_{jk}^{[i]} &\simeq \tilde{W}_{ik}^{[j]} \simeq \tfrac{1}{2}\tilde{W}_{lk}^{[ij]} \,, \end{aligned} \tag{5.90}$$

where $\tilde{W}_{lk}^{[ij]}$ has the following meaning after averaging over the azimuthal angle with respect to l:

$$\begin{aligned} \tilde{W}_{lk}^{[ij]} &= W_{lk}^{[l]} \quad \text{for } \theta_{lq} > \theta_{ij} \\ &= 0 \quad \text{for } \theta_{lq} < \theta_{ij} \,. \end{aligned} \tag{5.91}$$

Putting everything together, we can write Eq. (5.88) in this approximation as

$$W \simeq \boldsymbol{Q}_i^2 W_{ij}^{[i]} + \boldsymbol{Q}_j^2 W_{ij}^{[j]} + \boldsymbol{Q}_k^2 W_{lk}^{[k]} + \boldsymbol{Q}_l^2 \tilde{W}_{lk}^{[ij]} \,. \tag{5.92}$$

Eq. (5.92) has a simple interpretation: each of the partons i, j and k radiates in proportion to its colour charge squared. When i and j are close in angle, their incoherent contributions are limited (after azimuthal averaging) to cones of half-angle θ_{ij}. At larger angles, out to the direction of k, they give a coherent contribution in proportion to their combined colour charge squared, $\boldsymbol{Q}_l^2$. This contribution can be computed as if it came from an internal line of momentum $p_l = p_i + p_j$, but in reality it comes coherently from the two external lines.

The above treatment can be extended to higher orders, leading to a *coherent parton branching* formalism that can be used to compute soft gluon

Downloaded from https://www.cambridge.org/core. UNIVERSIDAD AUTONOMA METROPOLITANA, on 18 Nov 2026 at 04:36:53, subject to the Cambridge Core terms of use, available at https://www.cambridge.org/core/terms. https://doi.org/10.1017/CBO9780511628788.006

enhancements to all orders. The rules for coherent branching involve a simple modification of those for the collinear branching process considered earlier: in place of the virtual mass-squared variable t, we should use as evolution variable the opening angle θ, or more precisely the variable

$$\zeta = \frac{p_b \cdot p_c}{E_b E_c} \simeq 1 - \cos\theta \tag{5.93}$$

for the branching $a \to bc$, and impose angular ordering $\zeta' < \zeta$ where ζ and ζ' refer to successive branchings. The propagator factor dt/t in Eq. (5.28) is replaced by $d\zeta/\zeta$. Each parton radiates in proportion to its colour charge squared. In fact, if we use the appropriate splitting function $\hat{P}(z)dz$ in place of the soft approximation $\boldsymbol{Q}_a^2 d\omega/\omega$, the same formalism treats correctly both soft and collinear enhancements. Thus the basic formula for coherent branching becomes

$$d\sigma_{n+1} = d\sigma_n \frac{d\zeta}{\zeta} dz \frac{\alpha_s}{2\pi} \hat{P}_{ba}(z) \,. \tag{5.94}$$

In place of the virtual mass-squared cut-off used to terminate the collinear branching process and to regulate its infra-red divergences, we need to introduce an angular cut-off ζ_0 for the coherent branching. Again, this is to some extent a matter of choice, depending on how we classify a parton emission as unresolvable. The simplest choice is of the form

$$\zeta_0 = t_0/E^2 \tag{5.95}$$

for a parton of energy E. Then t_0 can once again be taken to be the minimum mass-squared. For radiation from a particle i of finite mass-squared t_0, the radiation function (5.72) receives a diagonal contribution,

$$\begin{aligned} \frac{\omega^2 p_i \cdot p_j}{p_i \cdot q \, p_j \cdot q} &\to \omega^2 \left(\frac{p_i \cdot p_j}{p_i \cdot q \, p_j \cdot q} - \frac{p_i^2}{(p_i \cdot q)^2} \right) \\ &\simeq \frac{1}{\zeta} \left(1 - \frac{t_0}{E^2 \zeta} \right) , \end{aligned} \tag{5.96}$$

and so the angular distribution of radiation is indeed cut off at $\zeta_0 = t_0/E^2$.

With the cut-off prescription (5.95), the most convenient definition of the evolution variable is not ζ itself but rather

$$\tilde{t} = E^2 \zeta \geq t_0 \,. \tag{5.97}$$

When using this variable, we have to remember that the angular ordering condition $\zeta_b, \zeta_c < \zeta_a$ for the branching $a \to bc$ translates into

$$\tilde{t}_b < z^2 \tilde{t} \,, \quad \tilde{t}_c < (1-z)^2 \tilde{t} \tag{5.98}$$

where $\tilde{t} = \tilde{t}_a$ and $z = E_b/E_a$. Thus the cut-off condition on z becomes

$$\sqrt{t_0/\tilde{t}} < z < 1 - \sqrt{t_0/\tilde{t}} \,. \tag{5.99}$$

Downloaded from https://www.cambridge.org/core. UNIVERSIDAD AUTONOMA METROPOLITANA, on 18 Nov 2026 at 04:36:53, subject to the Cambridge Core terms of use, available at https://www.cambridge.org/core/terms. https://doi.org/10.1017/CBO9780511628788.006

Neglecting the masses of b and c, the virtual mass-squared of a and the transverse momentum of the branching are given by

$$t = z(1-z)\tilde{t}\,, \quad p_t^2 = z^2(1-z)^2\tilde{t}\,. \tag{5.100}$$

Thus for the coherent branching process, the Sudakov form factor of the quark, for example, takes the form

$$\tilde{\Delta}_q(\tilde{t}) = \exp\left\{-\int_{4t_0}^{\tilde{t}} \frac{dt'}{t'} \int_{\sqrt{t_0/t'}}^{1-\sqrt{t_0/t'}} \frac{dz}{2\pi}\alpha_S(z^2(1-z)^2t')\hat{P}_{qq}(z)\right\}\,. \tag{5.101}$$

At large $\tilde{t}$ this falls more slowly than the function (5.58), but still faster than any negative power of $\tilde{t}$. The slower fall implies less branching, which is due to the suppression of soft gluon emission by angular ordering.

5.6 Hadronization models

After the parton shower described in the previous sections has terminated, we are left with a set of partons with virtualities (virtual masses-squared) of the order of the cut-off scale t_0. From this point we enter the low momentum-transfer, long-distance regime in which non-perturbative effects become important. The most important of these effects is hadronization, which converts the partons into the observed hadrons. At present we only have models for the hadronization process. These models are discussed briefly in the present section.

In principle the shower cut-off t_0 is an arbitrary parameter, unconnected with hadronization, for which the intrinsic energy scale is presumably of order Λ. On the other hand, when t_0 is increased the parton shower is terminated earlier and there are less partons to hadronize, with higher virtualities. These more virtual partons should be capable of producing more hadrons. Thus the hadronization model should ideally have a parameter t_0 whose effect cancels when the parton shower and hadronization phases of jet fragmentation are combined. In practice, cancellation will be imperfect owing to deficiencies of the model, and t_0 becomes a parameter to be varied in optimizing agreement with experiment. The favoured values tend to be rather small (a few times Λ) when the parton shower is handled carefully, implying that an extrapolation of perturbation theory is a more reliable guide to physics at such scales than the existing hadronization models.

One general approach to hadronization, based on the observation that perturbation theory seems to work well down to rather low scales, is the hypothesis of *local parton-hadron duality* [5]. Here one supposes only that the flow of momentum and quantum numbers at the hadron level tends to follow the flow established at the parton level. Thus, for example, the

Downloaded from https://www.cambridge.org/core. UNIVERSIDAD AUTONOMA METROPOLITANA, on 18 Nov 2026 at 04:36:53, subject to the Cambridge Core terms of use, available at https://www.cambridge.org/core/terms. https://doi.org/10.1017/CBO9780511628788.006

flavour of the quark initiating a jet should be found in a hadron near the jet axis. The extent to which the hadron flow deviates from the parton flow reflects the irreducible smearing of order Λ due to hadron formation.

The simplest more explicit hadronization model [6] is the longitudinal phase space or 'tube' model,[3] in which a parton (or, more realistically, a colour-connected pair of partons) produces a jet of light hadrons which occupy a tube in (y, p_t)-space, where $y = \frac{1}{2}\ln[(E+p_z)/(E-p_z)]$ is rapidity and p_t is transverse momentum, both measured with respect to the direction of the initial parton. If the hadron density in this space is $\rho(p_t)$, the energy and momentum of a tube of rapidity length Y are

$$\begin{aligned} E &= \int_0^Y dy\, d^2p_t \rho(p_t) p_t \cosh y = \lambda \sinh Y \\ P &= \int_0^Y dy\, d^2p_t \rho(p_t) p_t \sinh y = \lambda(\cosh Y - 1) \sim E - \lambda \,, \end{aligned} \tag{5.102}$$

where $\lambda = \int d^2p_t \rho(p_t) p_t$ sets the hadronization scale. Notice that the jet momentum P receives a negative hadronization correction of relative order $\lambda/E = 2\lambda/Q$ for a two-jet configuration of total energy Q. Thus one generally expects hadronization effects to scale with energy like $1/Q$.

From Eqs. (5.102) we expect a mean-square hadronization contribution to jet masses of

$$\langle M^2 \rangle_{\text{had}} = E^2 - P^2 \sim \lambda Q \,. \tag{5.103}$$

Comparing the perturbative predictions for jet masses with experiment, one finds that a hadronization correction corresponding to

$$\lambda \sim 0.5 \text{ GeV} \tag{5.104}$$

is required. Note that this implies a fairly large jet mass, about 7 GeV at $Q \sim M_Z$, in addition to the perturbative contribution.

Consider for example the thrust distribution, discussed in Chapter 3. The thrust of a two-jet event is precisely the jet momentum divided by the jet energy, and therefore we expect a hadronization correction of $-2\lambda/Q$. The purely perturbative prediction for the mean value of the thrust is [7]

$$\langle T \rangle = 1 - 0.334\,\alpha_S - 1.02\,\alpha_S^2 + \mathcal{O}(\alpha_S^3) \,, \tag{5.105}$$

which implies that $\langle 1 - T \rangle \sim 0.055$ at $Q = M_Z$, assuming $\alpha_S(M_Z^2) \sim 0.12$. The value measured at LEP is $\langle 1 - T \rangle = 0.068 \pm 0.003$, the discrepancy of 0.013 ± 0.003 being in agreement with the expected non-perturbative contribution of $2\lambda/Q \sim 0.011$. Fig. 5.13 shows that the same formula, *viz.*

[3] This model is essentially the simplest version of the string model; we call it a tube to avoid confusion with the more sophisticated Lund string model discussed below.

Downloaded from https://www.cambridge.org/core. UNIVERSIDAD AUTONOMA METROPOLITANA, on 18 Nov 2026 at 04:36:53, subject to the Cambridge Core terms of use, available at https://www.cambridge.org/core/terms. https://doi.org/10.1017/CBO9780511628788.006

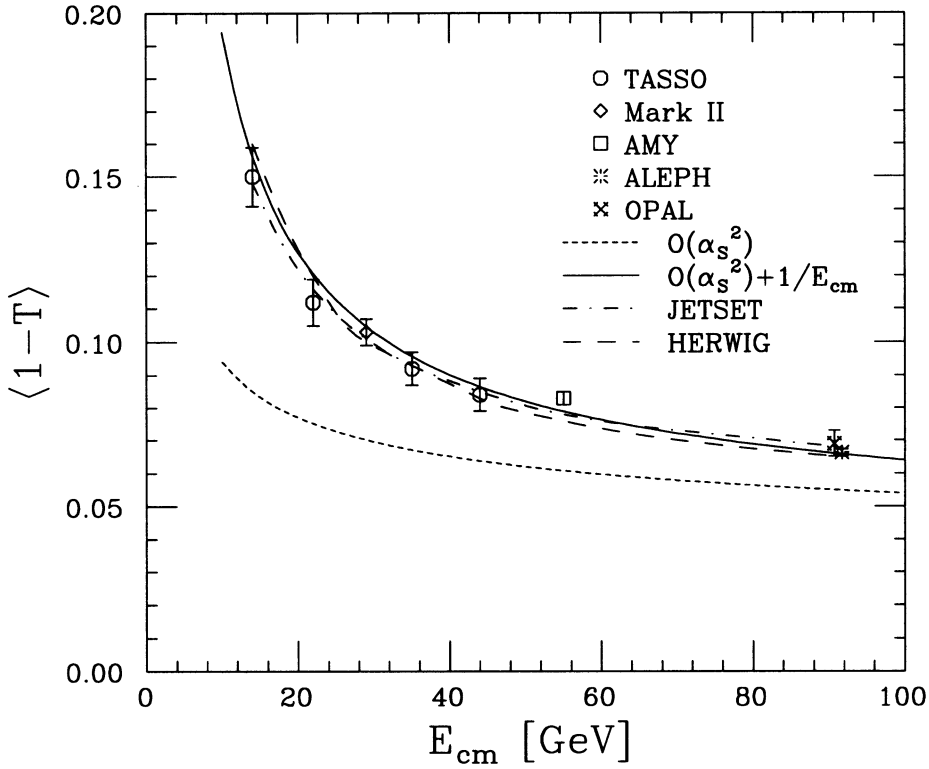


Fig. 5.13. $\langle 1 - T \rangle$, where T is the thrust, in e^+e^- annihilation.

the $\mathcal{O}(\alpha_S^2)$ perturbative prediction plus $2\lambda/Q = 1\ \text{GeV}/E_{\text{cm}}$, describes the energy dependence of $\langle 1 - T \rangle$ well down to $E_{\text{cm}} \sim 15$ GeV.

Also shown in Fig. 5.13 are the predictions of the QCD event generators HERWIG and JETSET, to be discussed in Section 5.7. It can be seen that the hadronization models built into these event generators also give rise to non-perturbative contributions of the required size and energy-dependence.

In order to make more detailed predictions, we need a specific model for the mechanism of hadronization. Over the years, three classes of models have been developed, which we outline briefly in the following subsections.

5.6.1 Independent fragmentation

The simplest scheme for generating hadron distributions from those of partons is to suppose that each parton fragments independently. The original approach of Field and Feynman [8] was designed to reproduce the limited transverse momenta and approximate scaling of energy frac-

Downloaded from https://www.cambridge.org/core. UNIVERSIDAD AUTONOMA METROPOLITANA, on 18 Nov 2026 at 04:36:53, subject to the Cambridge Core terms of use, available at https://www.cambridge.org/core/terms. https://doi.org/10.1017/CBO9780511628788.006

tion distributions observed in quark jets produced in e^+e^- annihilation at moderate energies. The fragmenting quark is combined with an antiquark from a $q\bar{q}$ pair created out of the vacuum, to give a 'first-generation' meson with energy fraction z. The leftover quark, with energy fraction $(1-z)$, is fragmented in the same way, and so on until the leftover energy falls below some cut-off. Scaling follows from the energy independence of the distribution assumed for z, which is known as the *fragmentation function*. The limited transverse momenta come from the relative transverse momenta of the created $q\bar{q}$ pairs, which are given a Gaussian distribution.

For gluon fragmentation, the gluon is first split into a $q\bar{q}$ pair, either assigning all the gluon's momentum to one or the other ($z = 0$ or 1) with equal probability [9], so that the gluon behaves as a quark of random flavour, or using the $g \to q\bar{q}$ Altarelli-Parisi splitting function [10].

With about four parameters to describe the fragmentation function, the width of the transverse momentum distribution, the ratio of strange to nonstrange pair creation, and the ratio of vector to pseudoscalar meson production, the model proved quite successful in describing the broad features of two-jet and three-jet final states in e^+e^- annihilation at moderate energies [9-11].

A weakness of the independent fragmentation scheme, as formulated above, is that the fragmentation of a parton is supposed to depend on its energy rather than its virtuality. Indeed, the fragmenting parton is usually assumed to remain on mass-shell, leading to violations of momentum conservation that have to be corrected by rescaling momenta after hadronization is completed. The residual colour and flavour of the leftover parton in each jet also have to be neutralized at this stage. There are further problems when jets become close together in angle. Instead of merging smoothly together into a single jet, as would happen if their fragmentation depended on their combined effective mass, even two precisely collinear jets remain distinguishable from a single jet.

5.6.2 String model

The string model of hadronization [12-14] is most easily described for e^+e^- annihilation. Neglecting for the moment the possibility of gluon bremsstrahlung, the produced quark and antiquark move out in opposite directions, losing energy to the colour field, which is supposed to collapse into a stringlike configuration between them. The string has a uniform energy per unit length, corresponding to a linear quark confining potential, which is consistent with quarkonium spectroscopy. The string breaks up into hadron-sized pieces through spontaneous $q\bar{q}$ pair production in its intense colour field.

In practice, the string fragmentation approach does not look very dif-

Downloaded from https://www.cambridge.org/core. UNIVERSIDAD AUTONOMA METROPOLITANA, on 18 Nov 2026 at 04:36:53, subject to the Cambridge Core terms of use, available at https://www.cambridge.org/core/terms. https://doi.org/10.1017/CBO9780511628788.006

ferent from independent fragmentation for the simple quark-antiquark system. The string may be broken up starting at either the quark or the antiquark end, or both simultaneously (the breaking points have space-like separations, so their temporal sequence is frame dependent), and it proceeds iteratively by $q\bar{q}$ pair creation, as in independent fragmentation. What one gains is a more consistent and covariant picture, together with some constraints on the fragmentation function [14], to ensure independence of whether one starts at the quark or the antiquark, and on the transverse momentum distribution [15], which is now related to the tunnelling mechanism by which $q\bar{q}$ pairs are created in the colour field of the string.

The string model becomes more distinct from independent fragmentation when gluons are present [16]. These are supposed to produce kinks on the string, each initially carrying localized energy and momentum equal to that of its parent gluon. The fragmentation of the kinked string leads to an angular distribution of hadrons in e^+e^- three-jet final states that is different from that predicted by independent fragmentation and in better agreement with experiment [17].

For multiparton states, such as those produced by the parton branching process at high Q^2, or for low values of the shower cut-off t_0, there is ambiguity about how strings should be connected between the various endpoints (quarks and antiquarks) and kinks (gluons). However, to leading order in N^{-2} where $N = 3$ is the number of colours, it is always possible to arrange the produced partons in a *planar* configuration, as discussed in Section 4.6.5. Then each has an equal and opposite colour to that of a neighbour (both neighbours, in the case of a gluon), like the quark and antiquark in the simplest e^+e^- final state. It seems most reasonable to stretch the string between these colour-connected neighbours. The reformulation of parton showers in terms of sequential splitting of colour dipoles [18] leads to the same prescription for string connection.

A schematic picture of the production of a multihadronic final state in e^+e^- annihilation according to the string model is shown in Fig. 5.14. Notice that whenever a gluon splits perturbatively into a quark-antiquark pair during the evolution of the parton shower, an additional string segment is produced. On the other hand, gluons which remain at the end of the shower (*i.e.* at the cut-off scale t_0) lead to kinks in the string segment which connects them. Each string segment then breaks up into hadrons as described above.

5.6.3 Cluster model

An important property of the parton branching process is the *preconfinement* of colour [19]. Preconfinement implies that the pairs of colour-

Downloaded from https://www.cambridge.org/core. UNIVERSIDAD AUTONOMA METROPOLITANA, on 18 Nov 2026 at 04:36:53, subject to the Cambridge Core terms of use, available at https://www.cambridge.org/core/terms. https://doi.org/10.1017/CBO9780511628788.006

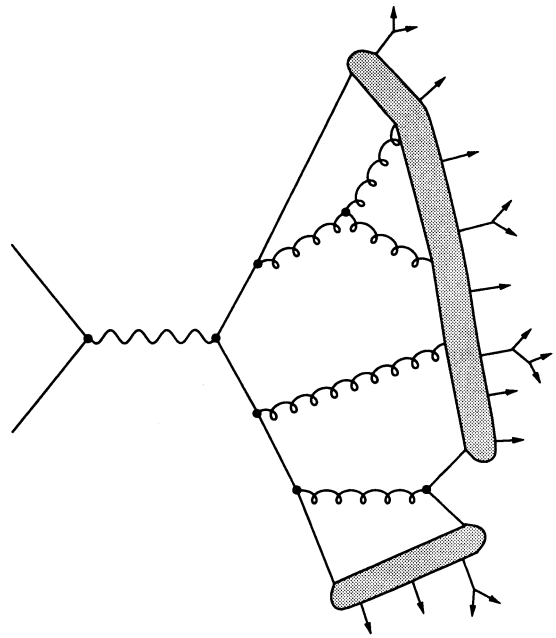


Fig. 5.14. Parton shower with string hadronization model for $e^+e^- \rightarrow$ hadrons.

connected neighbouring partons discussed above have an asymptotic mass distribution that falls rapidly at high masses and is asymptotically Q^2-independent and universal. This suggests a class of *cluster hadronization* models, in which colour-singlet *clusters* of partons form after the perturbative phase of jet development and then decay into the observed hadrons.

The simplest way for colour-singlet clusters to form after parton branching is through non-perturbative splitting of gluons into $q\bar{q}$ pairs [20]. Neighbouring quarks and antiquarks can then combine into singlets. The resulting cluster mass spectrum is again universal and steeply falling at high masses. Its precise form is determined by the QCD scale Λ, the cut-off scale t_0, and to a lesser extent the gluon-splitting mechanism. Typical cluster masses are normally two or three times $\sqrt{t_0}$.

If a low value of t_0 is used, of the order of 1 GeV^2 or less, most clusters have masses of up to a few GeV/c^2 and it is reasonable to treat them as superpositions of meson resonances. In a popular model [20,21], each such cluster is assumed to decay isotropically in its rest frame into a pair of hadrons, with branching ratios determined simply by density of states. The reduced phase space for cluster decay into heavy mesons and baryons is then sufficient to account for the multiplicities of the various kinds of hadrons observed in e^+e^- final states. Furthermore, the hadronic energy and transverse momentum distributions agree quite well with experiment,

Downloaded from https://www.cambridge.org/core. UNIVERSIDAD AUTONOMA METROPOLITANA, on 18 Nov 2026 at 04:36:53, subject to the Cambridge Core terms of use, available at https://www.cambridge.org/core/terms. https://doi.org/10.1017/CBO9780511628788.006

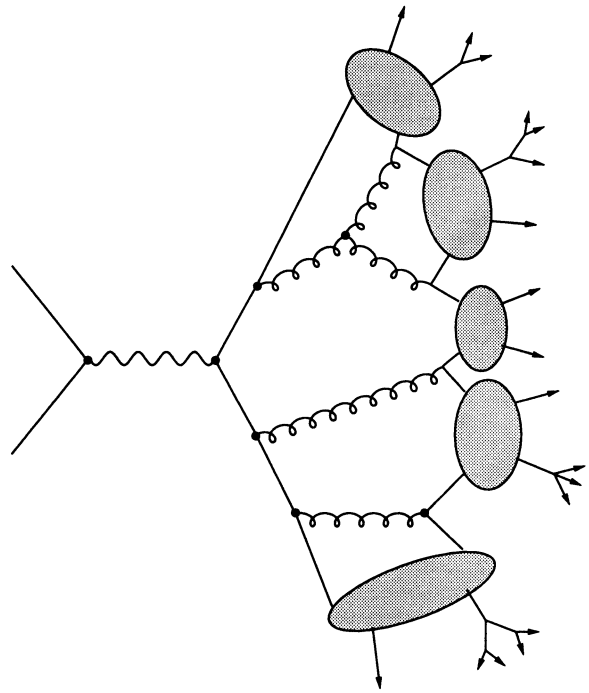


Fig. 5.15. Parton shower with cluster hadronization model for $e^+e^- \rightarrow$ hadrons.

without the introduction of any adjustable fragmentation functions. Also, the angular distribution in e^+e^- three-jet events is successfully described, as in the string model, provided soft gluon coherence is taken into account (see Section 5.5).

Fig. 5.15 shows the cluster hadronization of the same parton shower as in Fig. 5.14. The gluons that remain after the parton shower are split non-perturbatively into quark-antiquark pairs. The planar configuration of the shower determines that neighbouring pairs (not from the same gluon) can form colour-singlet mesonic clusters, which then undergo isotropic quasi-two-body decay into the observed hadrons.

An alternative approach to cluster formation and decay is to use a higher value of the cut-off t_0 and an anisotropic, multihadron decay scheme for the resulting heavy clusters [22]. Clearly, this approach lies somewhere between the low-mass cluster and string models. In practice, even with a low value of t_0 one needs to invoke a more complicated decay scheme for the small fraction of clusters that have masses of more than a few $\mathrm{GeV/c^2}$, for which isotropic two-body decay is an implausible hypothesis.

Downloaded from https://www.cambridge.org/core. UNIVERSIDAD AUTONOMA METROPOLITANA, on 18 Nov 2026 at 04:36:53, subject to the Cambridge Core terms of use, available at https://www.cambridge.org/core/terms. https://doi.org/10.1017/CBO9780511628788.006

5.7 QCD event generators

There are three classes of programs for generating full events from parton showers, using each of the three above-mentioned hadronization models.

Because of the difficulties discussed in connection with the independent fragmentation model, one would expect it to work best for the higher-momentum hadrons in final states consisting of a few well-separated jets. Probably on account of its simplicity, it was initially the model used most widely in conjunction with initial- and final-state parton branching for the simulation of hard hadron-hadron collisions, in the programs ISAJET [23], COJETS [24] and FIELDAJET [25].

The string hadronization model outlined above, with many further refinements, is the basis of the JETSET simulation program [26], which also includes final-state parton branching with optional angular ordering. This program gives a very good detailed description of hadronic final states in e^+e^- annihilation up to the highest energies studied so far.

The JETSET hadronization scheme is also used, in combination with initial- and final-state parton branching, in the other very successful Lund simulation programs PYTHIA [27] for hadron-hadron and LEPTO [28] for lepton-hadron collisions. The alternative formulation of parton showers in terms of colour dipole splitting mentioned above is implemented in the program ARIADNE [29], which also uses JETSET for hadronization.

The program HERWIG [4,30] uses a low-mass cluster hadronization model [21] in conjunction with initial- and final-state parton branching to simulate a wide variety of hard scattering processes. The branching algorithm includes angular ordering and azimuthal correlations due to coherence and gluon polarization. This approach gives a good account of diverse data with relatively few adjustable parameters.

Results from JETSET and HERWIG on the mean value of the thrust parameter are shown in Fig. 5.13. Both the string and cluster hadronization models lead a $1/E_{\rm cm}$ dependence of the non-perturbative contribution to this quantity, as seen in the data and in the simple 'tube' model discussed earlier.

References

1) J.D. Bjorken and S.D. Drell, *Relativistic Quantum Mechanics*, McGraw Hill, New York (1964).

2) D. Amati, A. Bassetto, M. Ciafaloni, G. Marchesini and G. Veneziano, *Nucl. Phys.* **B173** (1980) 429.

3) T. Sjöstrand, *Phys. Lett.* **B157** (1985) 321.

4) G. Marchesini and B.R. Webber, *Nucl. Phys.* **B310** (1988) 461.

5) Ya.I. Azimov, Yu.L. Dokshitzer, V.A. Khoze and S.I. Troyan, *Phys. Lett.* **B165** (1985) 147; *Zeit. Phys.* **C27** (1985) 65.

Downloaded from https://www.cambridge.org/core. UNIVERSIDAD AUTONOMA METROPOLITANA, on 18 Nov 2026 at 04:36:53, subject to the Cambridge Core terms of use, available at https://www.cambridge.org/core/terms. https://doi.org/10.1017/CBO9780511628788.006

6) R.P. Feynman, *Photon Hadron Interactions*, W.A. Benjamin, New York (1972).

7) Z. Kunszt, P. Nason, G. Marchesini and B.R. Webber, in 'Z Physics at LEP 1', CERN 89-08, vol. 1, p. 373.

8) R.D. Field and R.P. Feynman, *Phys. Rev.* **D15** (1977) 2590; *Nucl. Phys.* **B138** (1978) 1.

9) P. Hoyer *et al.*, *Nucl. Phys.* **B161** (1979) 349.

10) A. Ali *et al.*, *Phys. Lett.* **B93** (1980) 155.

11) A. Ali *et al.*, *Nucl. Phys.* **B168** (1980) 409.

12) X. Artru and G. Mennessier, *Nucl. Phys.* **B70** (1974) 93.

13) M.G. Bowler, *Zeit. Phys.* **C11** (1981) 169.

14) B. Andersson, G. Gustafson and B. Söderberg, *Zeit. Phys.* **C20** (1983) 317; *Nucl. Phys.* **B264** (1986) 29.

15) B. Andersson, G. Gustafson, G. Ingelman and T. Sjöstrand, *Phys. Rep.* **97** (1983) 33.

16) T. Sjöstrand, *Nucl. Phys.* **B248** (1984) 469.

17) JADE collaboration, W. Bartel *et al.*, *Phys. Lett.* **B157** (1985) 340;
TPC collaboration, H. Aihara *et al.*, *Zeit. Phys.* **C28** (1985) 31;
TASSO collaboration, M. Althoff *et al.*, *Zeit. Phys.* **C29** (1985) 29.

18) G. Gustafson, *Phys. Lett.* **B175** (1986) 453;
G. Gustafson and U. Pettersson, *Nucl. Phys.* **B306** (1988) 746.

19) D. Amati and G. Veneziano, *Phys. Lett.* **B83** (1979) 87;
A. Bassetto, M. Ciafaloni and G. Marchesini, *Phys. Lett.* **B83** (1979) 207;
G. Marchesini, L. Trentadue and G. Veneziano, *Nucl. Phys.* **B181** (1980) 335.

20) R.D. Field and S. Wolfram, *Nucl. Phys.* **B213** (1983) 65.

21) B.R. Webber, *Nucl. Phys.* **B238** (1984) 492.

22) T.D. Gottschalk, *Nucl. Phys.* **B214** (1983) 201.

23) F.E. Paige and S.D. Protopopescu, in Proc. UCLA Workshop, eds. H.-U. Bengtsson *et al.*, World Scientific, Singapore (1986).

24) R. Odorico, *Comp. Phys. Comm.* **32** (1984) 139; *ibid.* **59** (1990) 527.

25) R.D. Field, *Nucl. Phys.* **B264** (1986) 687.

26) T. Sjöstrand, *Comp. Phys. Comm.* **39** (1986) 347;
M. Bengtsson and T. Sjöstrand, *Comp. Phys. Comm.* **43** (1987) 367.

27) H.-U. Bengtsson and T. Sjöstrand, *Comp. Phys. Comm.* **46** (1987) 43;
T. Sjöstrand, *Comp. Phys. Comm.* **82** (1994) 74.

28) G. Ingelman, in Proc. Workshop on Physics at HERA, eds. W. Buchmüller and G. Ingelman, DESY, Hamburg (1991).

29) L. Lönnblad, *Comp. Phys. Comm.* **71** (1992) 15.

30) G. Marchesini, B.R. Webber, G. Abbiendi, I.G. Knowles, M.H. Seymour and L. Stanco, *Comp. Phys. Comm.* **67** (1992) 465.

Downloaded from https://www.cambridge.org/core. UNIVERSIDAD AUTONOMA METROPOLITANA, on 18 Nov 2026 at 04:36:53, subject to the Cambridge Core terms of use, available at https://www.cambridge.org/core/terms. https://doi.org/10.1017/CBO9780511628788.006